Computers and Structures 321 (2026) 108097

Contents lists available at ScienceDirect

Computers and Structures

journal homepage: www.elsevier.com/locate/cas

A framework for simulation-based transfer path analysis using dynamic substructuring and component mode synthesis

Said El Kadmiri Pedraza [a, b,*], Hans Peter Monner [a, b], Stephan Algermissen [a]

[a] Institute of Lightweight Systems, German Aerospace Center (DLR), Lilienthalplatz 7, 38108, Braunschweig, Germany
[b] Otto Von Guericke University Magdeburg, Universitätsplatz 2, 39106, Magdeburg, Germany

HIGHLIGHTS

- Development of a general framework to implement simulation-based Transfer Path Analysis using Component Mode Synthesis.
- Introduction of a new dual fixed-interface CMS method: Fixed Dual Craig-Bampton (FDCBM).
- Distinction of two TPA families: displacement-based (primal) and force- based (dual), and implementation of multilevel TPA.
- Free-interface CMS methods are inaccurate and computationally expensive in the studied example.
- The FDCBM competes with Craig-Bampton in accuracy and efficiency, and it emerges as the best candidate for force-based TPA.

ARTICLE INFO

Keywords:
Dynamic substructuring
Component mode synthesis
Transfer path analysis
Finite element model

ABSTRACT

This paper presents a simulation-based framework for Transfer Path Analysis (TPA) using Dynamic Substructuring (DS) and Component Mode Synthesis (CMS) in the context of Finite Element Analysis. A new CMS method is introduced, which combines fixed-interface and constraint modes within a dual assembly formulation, referred to as the Fixed-dual Craig-Bampton Method.

The framework enables the application of DS and CMS techniques for Multilevel TPA, offering a structured approach to trace vibration transmission through hierarchical vibrating sublevels. Two families of TPA are defined and investigated: displacement-based (primal) and force-based (dual). A detailed structural example is provided to benchmark several CMS methods and to evaluate the trade-offs between computational efficiency and accuracy in numerical TPA.

The results highlight the advantages of Multilevel TPA in isolating critical substructures. The benchmark analysis establishes the Craig-Bampton Method (primal) and the novel Fixed-dual Craig-Bampton Method (dual) as the most suitable CMS approaches for numerical TPA. Finally, displacement-based and force-based TPA results are compared. Both approaches exhibit different contribution results, leading to different interpretations of the Transfer Path Analysis.

1. Introduction

Dynamic Substructuring (DS) and Transfer Path Analysis (TPA) are closely related methodologies in structural dynamics. DS provides a means to divide a structural domain into subdomains, enforcing compatibility in terms of displacements and equilibrium in terms of forces [2]. On the other hand, TPA is focused on the determination of path contributions, and it also involves substructuring the problem. Transfer Path Analysis is primarily used in experimental testing to determine the main paths in existing assemblies (classical-TPA) or in models where the source of vibration is characterized (component-based TPA) [22].

These traditional TPA approaches consist of: 1) obtaining the characteristics of the receiver component using Frequency Response Functions (FRFs), normally represented as the admittances of the system, either measured in experimental testing or in numerical analyses, 2) obtaining the interface forces between the source component, generally in frequency domain, and 3) estimating the path contributions given the admittances and the interface forces. This procedure is also known as Frequency-Based Substructuring (FBS) [4].

* Corresponding author at: Institute of Lightweight Systems, German Aerospace Center (DLR), Lilienthalplatz 7, 38108, Braunschweig, Germany.
Email addresses: said.elkadmiripedraza@dlr.de (S. El Kadmiri Pedraza), Hans.Monner@dlr.de (H.P. Monner), Stephan.Algermissen@dlr.de (S. Algermissen).

https://doi.org/10.1016/j.compstruc.2026.108097
Received 30 June 2025; Accepted 3 January 2026
Available online 19 January 2026

Nomenclature

$*_b$, $*_{bb}$	Pertaining to interface DOF
$*_i$, $*_{ii}$	Pertaining to internal DOF
$*_j$	Pertaining to prescribed interface DOF
$*_k$	Pertaining to retained interface DOF
$*^{(P)}$	Pertaining to the passive assembly
$*^{(s)}$	Pertaining to the substructure
$\boldsymbol{A}_{bb}$	Equilibrium matrix applied to interface DOF
AP	Active-passive assembly
$\boldsymbol{B}$	Constraint matrix
$\boldsymbol{B}_{b,j}$	Selection matrix of prescribed DOF
$\boldsymbol{B}_{b,k}$	Selection matrix of retained DOF
$\boldsymbol{B}_{bb}$	Interface DOF selection matrix
$\boldsymbol{B}_{eq}$	Equilibrium matrix applied to assembly DOF
$\boldsymbol{B}_{ii}$	Internal DOF selection matrix
CBM	Craig-Bampton Method
CCBM	Condensed Craig-Bampton Method
CDCBM	Condensed dual Craig-Bampton Method
CMS	Component Mode Synthesis
$\boldsymbol{D}$	Damping matrix
DCBM	Dual Craig-Bampton Method
DOF	Degree of freedom
DS	Dynamic Substructuring
$\boldsymbol{f}$	Assembly force block-vector
f-TPA	Force-based TPA
FDCBM	Fixed dual Craig-Bampton Method
FRF	Frequency Response Function
$\boldsymbol{\Phi}$	Component modes
$\boldsymbol{\Phi}_i$	Internal component modes
$\boldsymbol{\Psi}_{ib}$	Constraint modes
$\boldsymbol{g}$	Assembly interface force block-vector
$\boldsymbol{G}_r$	Residual flexibility matrix
$\boldsymbol{K}$	Stiffness matrix
$\boldsymbol{L}$	Localization matrix
$\boldsymbol{\lambda}$	Vector of Lagrange Multipliers
$\boldsymbol{M}$	Mass matrix
MNM	MacNeal's Method
$\boldsymbol{\Omega}^2$	Component eigenvalues
$\boldsymbol{P}_i$	Passive assembly at i-th TPA level
RM	Rubin Method
TPA	Transfer Path Analysis
u-TPA	Displacement-based TPA
$\boldsymbol{u}$	Assembly displacement block-vector
$\boldsymbol{u}_b$	Vector of coupled interface DOF
$\boldsymbol{u}_{b,0}$	Vector of uncoupled interface DOF
$\boldsymbol{u}_m$	Modal participation vector
$\boldsymbol{u}_{m,i}$	Internal modal participation vector
$\boldsymbol{u}_p$	Prescription vector
$\boldsymbol{Y}, \boldsymbol{Z}$	Admittance, impedance

The Dynamic Substructuring formulation treated in the context of this paper is focused on analysing Finite Element Models. The DS approach and the Component Mode Synthesis (CMS) reductions have been extensively studied by many authors, and the work presented in this paper is based on the work by Allen, Rixen, de Klerk, and Gruber [2,6,9], as well as two recent formulations presented by the authors of this paper [7]. In the book [2], a compilation of the most relevant CMS methods was presented: namely the Craig-Bampton, Rubin, MacNeal and Dual Craig-Bampton methods. A previous two reviews, on which the book is based, correspond to [9], which compares different CMS methods and analyzes them from the point of view of sparsity patterns, and [6], which establishes a general framework for Dynamic Substructuring. In [7], the authors of this paper developed two CMS methods: the Condensed Craig-Bampton and the Condensed Dual-Craig Bampton. However, these works only tackle the substructuring problem to assemble independent subdomains, and they are not focused on performing TPA (Table 1).

As the authors of this paper are concerned, no structured methodology that links CMS with TPA exists, since the two formulations are essentially different in nature: CMS uses the impedances (or dynamic stiffnesses) of the components, while TPA requires the admittances (inverses of the impedances) to work. Furthermore, the CMS impedances are given by mass, damping and stiffness FEM matrices that are frequency independent, allowing for both time-domain and frequency-domain analyses, whereas the traditional TPA approach requires single Frequency Response Functions. This lack of connection between the methodologies has already been underlined by van der Seijs [22], even though early works done by Rubin [19] suggested a link between them. However, some works include TPA and simulation models that integrate DS or CMS in the analysis:

- In [15], the work presents an experimentally based CMS method for predicting the forced response of coupled substructures by combining test-derived models and uncoupled responses, enabling hybrid experimental–numerical analysis in the frequency domain.
- In [24], the study applies CMS for model order reduction in a multi-body simulation framework to analyze structure-borne sound transmission and transfer path behavior in a rail bogie system.
- In [1], the work presents a numerical TPA approach combining DS and flexible multibody simulation, where structure-borne noise paths are evaluated using the Wave Based Method (WBM) to assess excitation-response relationships in a 4-cylinder engine.
- In [11], the study combines FBS and blocked-force TPA to enable parametric NVH optimization, demonstrating a hybrid modeling approach for an electric compressor assembly with virtual coupling.
- In [16], the author applies simulation-based adaptations of classical and component-based TPA methods to elastic multi-body models, enabling efficient NVH analysis and weak spot detection in complex systems through accurate post-processing of numerical drivetrain simulations.
- In [13], excitation forces at the mounts are obtained from an FE model of the real powertrain, while the vehicle body–cavity FRFs are measured experimentally using vibro-acoustic reciprocity.
- The work in [8] explicitly frames the intersection of TPA and FBS, proposing a control-based hybrid substructuring approach to TPA.
- In [10], a transfer path model of a two-stage serial isolation system is developed combining FBS and DS.
- In [12], DS and FBS are again merged, where TPA is cast into a DS framework by using FRFs and virtual infinite-stiffness springs to numerically remove individual paths and evaluate their road-noise contribution without classical/operational TPA testing.
- In [23], TPA is performed through FBS by using elastic Multibody Simulation to compute path forces and FRFs, which are combined with experimental TPA sound-radiation FRFs to identify and optimize critical transfer paths.

These examples illustrate how DS and CMS, combined with FE and multibody models, are used within TPA, while the actual contribution analysis is consistently based on Frequency Based Substructuring relying on FRFs. Moreover, most studies focus on hybrid TPA, i.e., integrating

Table 1
Comparison between traditional (classical and component-based) TPA and the new DS/CMS-based TPA workflows.

Traditional TPA	DS/CMS-based TPA
General workflow: • Properties of Passive (P) and Active (A) components using **Frequency Response Functions (FRFs)** • Operational Forces: • Classical TPA: Contact forces in AP $\left(g_j^{(P)}\right)$ • Component-based TPA: Blocked-forces in A $\left(g_j^{eq}\right)$ • Estimation of *j-th* path contribution: • Classical TPA: $u_j^{(P)} = Y_j^{(P)} g_j^{(P)}$ • Component-based TPA: $u_j^{(P)} = Y_j^{(AP)} g_j^{eq}$	**General workflow:** • Properties of Passive and Active components using **Finite Element Model (FEM)** matrices (mass, stiffness, damping) • Operational Forces: Contact forces AP $g_j^{(P)}$ • Estimation of *j-th* path contribution: Solution of DS problem $M_j^{(P)}\ddot{u}_j^{(P)} + D_j^{(P)}\dot{u}_j^{(P)} + K_j^{(P)}u_j^{(P)} = g_j^{(P)}$
Key features: • Use of admittances $Y(\omega) = Z^{-1}(\omega)$ • Frequency-Based Substructuring (FBS) • Experimental or hybrid experimental-simulation set-ups. • Limited to small sets of FRFs and interfaces	**Key features:** • Use of FEM mass, damping, and stiffness matrices • Dynamic Substructuring and Component Mode Synthesis • Time-domain and frequency-domain • Fully simulation-based methodology

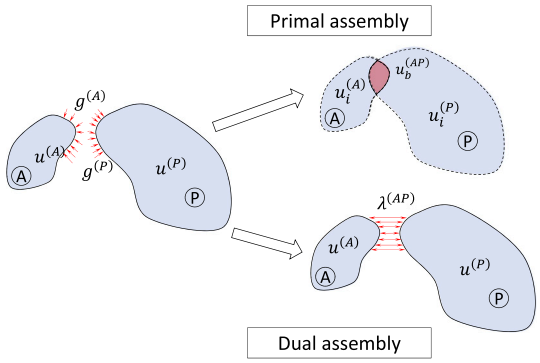

Fig. 1. Primal and dual assembly coupling. In the primal assembly, a common set of displacement DOF is established. In the dual assembly, the interface forces are part of the unknowns. The first approach integrates compatibility and equilibrium, and in the second compatibility is imposed explicitly.

numerical and experimental analyses. In contrast, the approach in this article is fully numerical and implemented entirely within FE models.

Integrating TPA within the framework of DS and CMS enables the formulation of new methodological strategies. The application of the primal assembly (see Fig. 1) in TPA leads to a formulation where interface displacements are imposed. This differentiation leads to the classification of two TPA families: displacement-based TPA (primal), and force-based TPA (dual).

The new TPA representation makes it easier to perform complex analyses, since the procedure can be carried out systematically in a numerical scheme. Within this framework, the hierarchical extension of TPA, referred to as multilevel TPA [21], is introduced at the context of DS to analyze paths in different active-passive levels.

The force-based traditional TPA methodologies are focused on analysing forces at the interfaces between the components. From the DS approach, this involves the computation of interface forces, which requires a *dual* formulation. The problem with the dual methods is that they require solving for larger systems of equations than primal methods, since they also include interface forces as unknowns, which represent a larger number of degrees of freedom (DOF). For this purpose, CMS reduces the computational needs.

However, the authors of this paper have shown in a recent work [7] that the CMS methods aimed at tackling the dual problem (Dual Craig-Bampton [18] and Condensed dual Craig-Bampton [7]) are not accurate enough to assemble the models. There is a need for a solid dual CMS method for the development of a CMS-TPA methodology.

This paper addresses the previous research frontiers by:

- Establishing a common framework to apply TPA from a Finite Element modeling perspective. It formalizes how primal and dual assemblies in Dynamic Substructuring, as well as fixed-interface and free-interface CMS methods, can be efficiently applied to study TPA using FE-based numerical models.
- Introducing a new dual CMS method based on the concepts of fixed-interface and constraint modes. It aims to provide a reliable CMS method to compute interface forces.
- Integrating the new TPA methodology into the Multilevel TPA paradigm.
- Analyzing the differences between displacement-based TPA, based on primal methods, and force-based TPA, based in dual methods.

And it introduces the following advances over the existing literature:

- A systematic and fully numerical TPA methodology that operates directly on simulation models without computing and evaluating FRFs, providing a new interpretation of the TPA paradigm — traditionally tied to Frequency Based Substructuring, with admittances — now consistently embedded within standard FE analyses.
- A dual CMS formulation specifically designed to overcome the accuracy limitations reported for previous dual CMS approaches.

The novel TPA methodology is validated with an analytical multi mass-spring system. All the methodologies introduced in the paper are demonstrated through a numerical example. This example is used to establish which CMS method is more appropriate for the TPA problem, as well as to study the advantages of using Multilevel TPA, and to highlight the variability of contribution results when using a primal method (displacement-based TPA) and a dual method (force-based TPA).

2. The transfer path problem

Transfer Path Analysis aims to identify and quantify the transmission of forces and vibrations between interconnected substructures. While traditional TPA primarily relies on experimental measurements and Frequency Response Functions, a Dynamic Substructuring perspective offers a computationally efficient approach to model and analyze transfer paths within numerical simulations.

Consider a coupled dynamic system composed of two subsystems, A (active) and P (passive), which are interconnected at a shared interface (see Fig. 2). The dynamic behavior of this assembly can be described

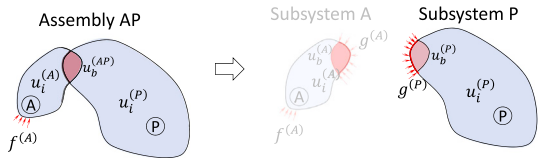

Fig. 2. Representation of the transfer path problem in the context of dynamic substructuring. the system is decomposed into an active and a passive part. The subsystem A is substituted in subsystem P by the interface forces and interface displacements generated at the active-passive interface.

in terms of internal degrees of freedom within each subsystem and interface DOFs, where forces and displacements are transmitted. In this framework:

- The operational excitation occurs in subsystem A.
- The transmission path is characterized by the interface forces or displacements in the shared interface.
- The response at subsystem P results from the interface forces and imposed displacements originating in the assembly AP.

Through this approach, transfer path contributions can be systematically analyzed using different CMS techniques as dynamic substructuring reduction methods. The interface forces can be reconstructed using dual assembly formulations, whereas interface displacements can be obtained through primal methods. The methodology described in this work establishes a Numerical Transfer Path Analysis, allowing for:

- The application of reduced-order substructuring techniques to efficiently compute transfer paths.
- A force-based interpretation using dual assembly methods, directly linking interface forces to receiver responses.
- A displacement-based interpretation using primal assembly methods, prescribing interface displacements to the receiver responses.

3. Multilevel TPA

Multilevel Transfer Path Analysis extends conventional TPA by systematically evaluating the contribution of components across multiple hierarchical subsystem levels, forming a “chain” of interconnected subsystems [21]. This approach is particularly useful in complex structures where vibrations propagate through multiple intermediate components before reaching the target response location.

The fundamental principle of Multilevel TPA is the decomposition of a global dynamic system into successive subsystem levels. Each subsystem is characterized by a subset of components, a set of external interfaces and a set of internal interfaces.

Fig. 3 depicts the general workflow of Multilevel TPA in the context of DS. In the first level, the load is applied to the active component A, and the interface forces or interface displacements are computed across the entire assembly. The interface DOF are used as input to the following level. This process is performed from the *Level 0* (active-passive assembly AP) to the *Level n*, which is physically the ultimate receiver. By cascading the interface forces and displacements across different levels, the multilevel transmission paths are obtained, linking the original excitation source to the final target response. This process can generate a diverse network of transfer paths, as it is depicted in Fig. 4.

Multilevel TPA offers a systematic workflow for assessing noise and vibration propagation, enabling the identification of contributions from individual components across multiple hierarchical levels. However, compared to the traditional one-level TPA approach, the number of potential transfer paths increases exponentially, making exhaustive analysis computationally demanding. For this, reduction techniques in Dynamic Substructuring significantly enhance computational efficiency, allowing the evaluation of a large number of transfer paths that would otherwise be impractical.

4. Dynamic substructuring for numerical Transfer Path Analysis

This section introduces different Dynamic Substructuring and Component Mode Synthesis methods and the derivation of them from a common framework. A summary of these methods can be observed in Table 2. In this section, the work done by Allen, Rixen, de Klerk and Gruber [2,6,9] in compiling the different CMS methods is presented, shaped for the application to Numerical Transfer Path Analysis. A new method is also introduced in this section, in the framework of fixed-interface methods for dual assembly: a Fixed-Dual Craig-Bampton.

Consider a Finite Element Model of a global domain that is decomposed into N non-overlapping substructures. In this partitioning, each node is associated with a single substructure, except for those located at the interface boundaries, which are shared between adjacent substructures.

The linear or linearized equation of motion for an undamped substructure is formulated as:

$$M^{(s)}\ddot{u}^{(s)} + K^{(s)}u^{(s)} = f^{(s)} + g^{(s)} \tag{1}$$

where the superscript (s) designates a specific substructure. The parameters $M^{(s)}$ and $K^{(s)}$ represent the mass and stiffness matrices, respectively, while $u^{(s)}$ denotes the displacement vector (degrees of freedom, DOF) of the substructure. The equation is excited by the external force vector $f^{(s)}$ and the interface force vector $g^{(s)}$, the latter arising from interactions between adjacent substructures.

By assembling all $N^{(P)}$ substructures contained in assembly P, the equations of motion can be expressed in a block-diagonal form as:

$$M^{(P)}\ddot{u}^{(P)} + K^{(P)}u^{(P)} = f^{(P)} + g^{(P)} \tag{2}$$

where $M^{(P)}$ and $K^{(P)}$ are the uncoupled global mass and stiffness matrices, $u^{(P)}$ is the global uncoupled displacement vector, and $f^{(P)}$ and $g^{(P)}$ are the global external and interface force vectors, respectively. The format of these matrices can be found in [6] or [9]. For simplicity, the super-index P indicating that it corresponds to the assembly P will be avoided from now on.

The assembly process enforces two essential conditions: (1) compatibility of interface degrees-of-freedom (DOF) at the interface and (2) equilibrium of interface forces. The compatibility condition is formulated using a constraint matrix B, which ensures continuity of DOF at adjacent interfaces by selecting the corresponding interface DOF pairs for each subdomain and establishing opposite signs for each side of the connected substructures [2]:

$$Bu = 0 \tag{3}$$

Similarly, the equilibrium condition is expressed through the localization matrix L. This localization matrix enforces g to be zero within the internal subset, and sets equilibrium at the connecting interfaces:

$$L^T g = 0 \tag{4}$$

The localization matrix L is constructed using selection matrices that differentiate between internal and interface DOF within each substructure, along with the interface compatibility matrix:

$$L = \begin{bmatrix} B_{ii}^T & B_{bb}^T A_{bb}^T \end{bmatrix} = \begin{bmatrix} B_{ii}^T & B_{eq}^T \end{bmatrix} \tag{5}$$

where B_{ii} and B_{bb} are selection matrices for internal and interface nodes of each substructure, respectively. The interface selection matrix B_{bb} differs from the constraint matrix B in the feature of only selecting interface DOF, maintaining the original signs at both sides and not establishing any connection condition between the substructures. The matrix A_{bb} establishes a common set of interface displacements applied to the uncoupled interface DOF set $u_{b,0}$, while B_{eq} enforces this condition in the

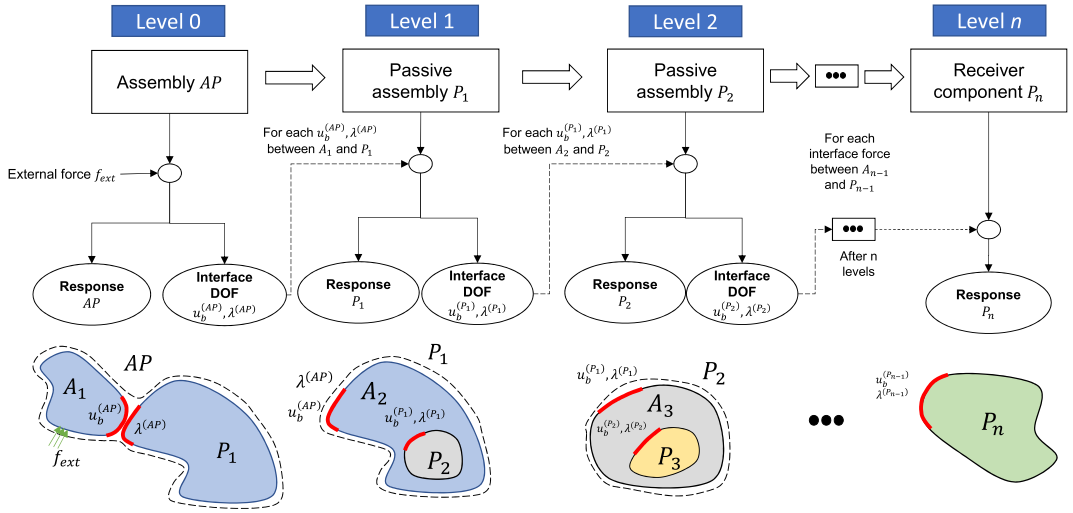

Fig. 3. Representation of the multilevel transfer path problem in the context of dynamic substructuring. The system is systematically decomposed into active and passive parts throughout different levels. In every level, the interface forces or displacements from the previous level are studied as external excitations.

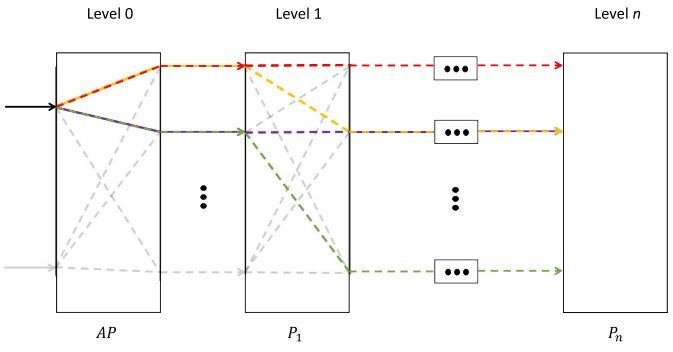

Fig. 4. Multilevel TPA network. From assembly AP to receiver system P_n.

global set u, and it is equivalent to $|B|$. It can be demonstrated that the matrix A_{bb} is obtained as:

$$A_{bb} = (B_{bb}B_{bb}^T)^{-1} \tag{6}$$

It is important to note that this procedure is specifically tailored for conformal meshes, but it can be extended to non-conformal meshes with some modifications of the connection matrices $B_{bb}, A_{bb}, B, B_{eq}$.

The equation of motion (2), the compatibility condition (3) and the equilibrium condition (4) can be written in a single equation system, which constitutes the dynamic substructuring statement.

$$\begin{cases} M\ddot{u} + Ku = f + g, & \text{equation of motion} \\ Bu = 0, & \text{compatibility} \\ L^T g = 0, & \text{equilibrium} \end{cases} \tag{7}$$

From here, two routes can be derived: a primal route, which reduces the DS problem to the displacement DOF, and a dual route, which solves all displacement DOF together with the interface forces between components. In this paper, these two routes will be studied separately and further transformations to reduce the size of the systems will be performed.

4.1. Primal assembly

In this subsection, the primal assembly approach is addressed and adapted to apply Numerical Transfer Path Analysis. Further transformations are performed using fixed and free-interface Component Mode Synthesis (CMS) methods, together with a modal reduction of the primal assembly.

In the primal assembly approach, the compatibility condition is *a priori* satisfied by using a common set of interface displacements. For that, an initial transformation from the global u to internal u_i and uncoupled interface $u_{b,0}$ displacement vectors is needed:

$$u = \begin{bmatrix} B_{ii}^T & B_{bb}^T \end{bmatrix} \begin{bmatrix} u_i \\ u_{b,0} \end{bmatrix} = T_0 \begin{bmatrix} u_i \\ u_{b,0} \end{bmatrix} \tag{8}$$

Table 2
Dynamic Substructuring and Component Mode Synthesis methods studied in this paper.

	Dynamic Substructuring					
			Component Mode Synthesis			
	Full	Reduced	Fixed-methods		Free-methods	
			Full	Reduced	Full	Reduced
Primal	Physical	Modal	Craig-Bampton	Condensed Craig-Bampton	Rubin	MacNeal
Dual	Physical		Fixed Dual Craig-Bampton		Dual Craig-Bampton	Condensed Dual Craig-Bampton

with B_{ii} and B_{bb} the same matrices as in the equilibrium Eq. (4). A further transformation can be done to establish the unique set of interface displacements u_b:

$$\begin{bmatrix} u_i \\ u_{b,0} \end{bmatrix} = \begin{bmatrix} I & 0 \\ 0 & A_{bb}^T \end{bmatrix} \begin{bmatrix} u_i \\ u_b \end{bmatrix} = T_1 \begin{bmatrix} u_i \\ u_b \end{bmatrix} \tag{9}$$

with A_{bb} defined as in (4). Notice that the localization matrix L is the product of T_0 and T_1. This unique set of interface displacements automatically satisfies the compatibility condition (3), resulting in L as the nullspace of B.

$$Bu = BL \begin{bmatrix} u_i \\ u_b \end{bmatrix} = 0, \quad \forall \begin{bmatrix} u_i \\ u_b \end{bmatrix} \neq 0 \tag{10}$$

The set of interface displacements u_b can be divided into *retained* ($u_{b,k}$) and *prescribed* ($u_{b,j}$). To better understand this separation, consider that the assembly contains active-passive and passive-passive interfaces. The active-passive interfaces connect the assembly P with the assembly A, in what was formed as the assembly AP (see Fig. 2). The passive-passive interfaces lie within the passive assembly P, and connect the different substructures contained.

The active-passive interface DOF are referred to here as the *prescribed* DOF ($u_{b,j}$), and the passive-passive are referred to as *retained* ($u_{b,k}$). The following transformation allows one to work in a more structured way with the prescribed interface conditions at the active-passive interfaces

$$\begin{bmatrix} u_i \\ u_b \end{bmatrix} = \begin{bmatrix} I & 0 & 0 \\ 0 & B_{b,k} & B_{b,j} \end{bmatrix} \begin{bmatrix} u_i \\ u_{b,k} \\ u_{b,j} \end{bmatrix} = T_2 \begin{bmatrix} u_i \\ u_{b,k} \\ u_{b,j} \end{bmatrix} \tag{11}$$

with $B_{b,k}$ and $B_{b,j}$ matrices that select the *retained* and *prescribed* interface DOF from the global interface displacement set u_b. The primal subspace projection can be obtained using the previous transformations as:

$$u = T_0 T_1 T_2 \begin{bmatrix} u_i \\ u_{b,k} \\ u_{b,j} \end{bmatrix} = T_{pr} \begin{bmatrix} u_i \\ u_{b,k} \\ u_{b,j} \end{bmatrix} \tag{12}$$

The equation of motion (2) of N substructures can be projected onto the subspace associated to u_i,$u_{b,k}$ and $u_{b,j}$, as defined by T_{pr} of Eq. (12). This equation already satisfies the compatibility and equilibrium conditions, which means that it is equivalent to the dynamic substructuring statement (7):

$$M_{pr} \begin{bmatrix} \ddot{u}_i \\ \ddot{u}_{b,k} \\ \ddot{u}_{b,j} \end{bmatrix} + K_{pr} \begin{bmatrix} u_i \\ u_{b,k} \\ u_{b,j} \end{bmatrix} = T_{pr}^T f \tag{13}$$

With the primal mass and stiffness matrices obtained as:

$$M_{pr} = \begin{bmatrix} M_{ii} & M_{ik} & M_{ij} \\ M_{ki} & M_{kk} & M_{kj} \\ M_{ji} & M_{jk} & M_{jj} \end{bmatrix} = T_{pr}^T M T_{pr}, \quad K_{pr} = \begin{bmatrix} K_{ii} & K_{ik} & K_{ij} \\ K_{ki} & K_{kk} & K_{kj} \\ K_{ji} & K_{jk} & K_{jj} \end{bmatrix} = T_{pr}^T K T_{pr} \tag{14}$$

The equation of motion in primal assembly (13) is in physical representation, expanding all the degrees-of-freedom of the entire assembly. Solving it requires high demand for computational resources, and it is sometimes referred to as the *direct solution* or *full solution*.

4.1.1. Modes of primal assembly

Solving the equation of motion in primal assembly (13) can be computationally expensive. To avoid this, a common approach is to reduce the system of equations by using a truncated set of the first modes of the assembly [3]. To achieve this, the Eq. (13) needs to be solved as an eigenvalue problem.

$$K_{pr}\varphi_{pr} = \omega^2 M_{pr}\varphi_{pr} \tag{15}$$

With ω and φ_{pr} the pair of natural frequency and mode shape in free-vibration. The displacements can be approximated using a truncated set of mode shapes Φ_{pr}:

$$\begin{bmatrix} u_i \\ u_{b,k} \\ u_{b,j} \end{bmatrix} \simeq \begin{bmatrix} \Phi_{pr,i} \\ \Phi_{pr,k} \\ \Phi_{pr,j} \end{bmatrix} u_m = \Phi_{pr} u_m \tag{16}$$

with the subindices *i, k, j* corresponding to the internal, *retained* interface and *prescribed* interface sets. For Numerical Transfer Path Analysis, the subset $u_{b,j}$ is prescribed, which means that the transformation (16) can be modified to keep $u_{b,j}$ as an additional unknown:

$$\begin{bmatrix} u_i \\ u_{b,k} \\ u_{b,j} \end{bmatrix} \simeq \begin{bmatrix} \Phi_{pr,i} & 0 \\ \Phi_{pr,k} & 0 \\ 0 & I \end{bmatrix} \begin{bmatrix} u_m \\ u_{b,j} \end{bmatrix} = T_3 \begin{bmatrix} u_m \\ u_{b,j} \end{bmatrix} \tag{17}$$

The modal subspace projection of the primal assembly can be obtained using the following transformation matrix:

$$u \simeq T_{pr} T_3 \begin{bmatrix} u_m \\ u_{b,j} \end{bmatrix} = T_{pr,m} \begin{bmatrix} u_i \\ u_{b,j} \end{bmatrix} \tag{18}$$

And the primal assembly equation of motion (13) can be transformed onto the truncated modal basis:

$$M_{pr,m} \begin{bmatrix} \ddot{u}_m \\ \ddot{u}_{b,j} \end{bmatrix} + K_{pr,m} \begin{bmatrix} u_m \\ u_{b,j} \end{bmatrix} = T_{pr,m}^T f \tag{19}$$

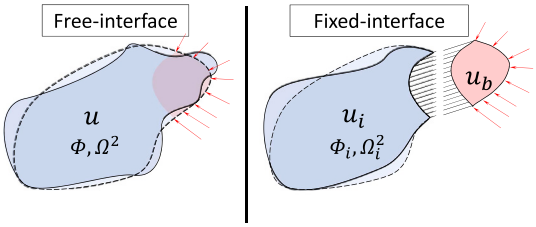

Fig. 5. Free-interface and fixed-interface modal reduction strategies. Free-interface methods use the modes of the entire set of DOF of each component and a static correction at connected interfaces. Fixed-interface methods, instead use the modes of the internal DOF and connects the components by constraint modes.

4.1.2. Primal fixed-interface Component Mode Synthesis methods

The concept of Component Mode Synthesis is inherited from Dynamic Substructuring. The key idea behind CMS is to assemble substructures by using a reduced representation of them, typically given by their first eigenmodes. This results onto the projection of the equation of motion in a reduced subspace that generally contains a smaller number of DOF.

Fixed-interface CMS refers to methods that use internal (fixed-interface) modes and constraint modes (see Fig. 5). As the author acknowledges, there are two main methods: Craig-Bampton [5] and Condensed Craig-Bampton Method [7].

Craig-Bampton method. The Craig-Bampton Method (CBM) [5] approximates the internal displacements by internal modes Φ_i and constraint modes Ψ_{ib}. The following equation adapts the CBM to the representation

of *retained* and *prescribed* interface sets:

$$\begin{bmatrix} u_i \\ u_{b,k} \\ u_{b,j} \end{bmatrix} \approx \begin{bmatrix} \Phi_i & \Psi_{ib,k} & \Psi_{ib,j} \\ 0 & I & 0 \\ 0 & 0 & I \end{bmatrix} \begin{bmatrix} u_{m,i} \\ u_{b,k} \\ u_{b,j} \end{bmatrix} = T_4 \begin{bmatrix} u_i \\ u_{b,k} \\ u_{b,j} \end{bmatrix} \tag{20}$$

where the internal modes Φ_i can be obtained by solving the internal eigenvalue problem of each substructure s and selecting a truncated set of modes

$$K_{ii}^{(s)} \varphi_i^{(s)} = \omega^2 M_{ii}^{(s)} \varphi_i^{(s)} \tag{21}$$

and $K_{ii}^{(s)}$, $M_{ii}^{(s)}$ are the entries corresponding to the internal DOF of substructure s as expressed in (14). By definition, K_{ii} and M_{ii} are block-diagonal matrices containing the internal terms of all N structures. The internal mode matrix Φ_i is also a block-diagonal matrix containing the truncated set of internal modes of each substructure. The constraint modes $\Psi_{ib,k}, \Psi_{ib,j}$ associated to the *retained* and *prescribed* interface DOF are obtained by solving the first line of the equation of motion in primal assembly (13) in static condition when it is only excited by interface displacements $u_{b,k}, u_{b,j}$. This means that the second order terms of the differential equation $\ddot{u}_i, \ddot{u}_{b,k}, \ddot{u}_{b,j}$ and the external force f are zero, resulting in the following definition:

$$\Psi_{ib,k} = -K_{ii}^{-1} K_{ik}, \quad \Psi_{ib,j} = -K_{ii}^{-1} K_{ij} \tag{22}$$

With K_{ik} and K_{ij} being the components of the primally assembled stiffness matrix (14) that correspond to the *retained* and *prescribed* DOF, respectively. The computation of constraint modes involves the inversion of each component internal stiffness matrix. These matrices are generally invertible, because the DOF of the interfaces are suppressed, equivalently to fixing them. Even when the stiffness matrices are sparse, their inverses can turn into dense matrices, which can increase the memory allocation [7].

The Craig-Bampton transformation can be obtained from the primal assembly transformation as a concatenation of T_{pr} with T_4:

$$u \simeq T_{pr} T_4 \begin{bmatrix} u_{m,i} \\ u_{b,k} \\ u_{b,j} \end{bmatrix} = T_{CB} \begin{bmatrix} u_{m,i} \\ u_{b,k} \\ u_{b,j} \end{bmatrix} \tag{23}$$

where $u_{m,i}$ is the vector of modal internal participation factors associated to each component. Transformation of the equation of motion (2) onto the Craig-Bampton reduction basis results:

$$M_{CB} \begin{bmatrix} \ddot{u}_{m,i} \\ \ddot{u}_{b,k} \\ \ddot{u}_{b,j} \end{bmatrix} + K_{CB} \begin{bmatrix} u_{m,i} \\ u_{b,k} \\ u_{b,j} \end{bmatrix} = T_{CB}^T f \tag{24}$$

The equation of motion, as in the primal assembly, enforces equilibrium of forces at the interfaces. It is a reduced system of equations because the number of DOF is reduced respect to the primal assembly.

Condensed Craig-Bampton method. A further reduction of the Craig-Bampton Method can be performed to obtain the Condensed Craig-Bampton Method (CCBM) [7]. For this, take the second line of the equation of motion in primal assembly (13) and substitute u_i with the approximation given by internal and constraint modes (20) along with the assumption that there is no external force being applied at the interface:

$$\begin{aligned} M_{ki}\Phi_i \ddot{u}_{m,i} + (M_{ki}\Psi_{ib,k} + M_{kk})\ddot{u}_{b,k} + (M_{ki}\Psi_{ib,j} + M_{kj})\ddot{u}_{b,j} \\ + K_{ki}\Phi_i u_{m,i} + (K_{ki}\Psi_{ib,k} + K_{kk})u_{b,k} + (K_{ki}\Psi_{ib,j} + K_{kj})u_{b,j} \simeq 0 \end{aligned} \tag{25}$$

In this equation, the following inertial terms can be neglected:

$$M_{ki}\Phi_i \ddot{u}_{m,i} \approx 0, \quad (M_{ki}\Psi_{ib,k} + M_{kk})\ddot{u}_{b,k} \approx 0, \quad (M_{ki}\Psi_{ib,j} + M_{kj})\ddot{u}_{b,j} \approx 0 \tag{26}$$

The second line of the primal equation of motion with internal and constraint modes (25) can be simplified and the *retained* interface DOF $u_{b,k}$ can be expressed in terms of $u_{m,i}$ and $u_{b,j}$:

$$u_{b,k} \simeq -(K_{ki}\Psi_{ib,k} + K_{kk})^{-1} \begin{bmatrix} K_{ki}\Phi_i & K_{ki}\Psi_{ib,j} + K_{kj} \end{bmatrix} \begin{bmatrix} u_{m,i} \\ u_{b,j} \end{bmatrix} = \begin{bmatrix} \Pi_{km} & \Pi_{kj} \end{bmatrix} \begin{bmatrix} u_{m,i} \\ u_{b,j} \end{bmatrix} \tag{27}$$

With this approximation, the DOF of the Craig-Bampton method can be expressed only as a linear combination of $u_{m,i}$ and $u_{b,j}$, reducing the system by the number of DOF of the *retained* interface DOF $u_{b,k}$.

$$\begin{bmatrix} u_{m,i} \\ u_{b,k} \\ u_{b,j} \end{bmatrix} \simeq \begin{bmatrix} I & 0 \\ \Pi_{km} & \Pi_{kj} \\ 0 & I \end{bmatrix} \begin{bmatrix} u_{m,i} \\ u_{b,j} \end{bmatrix} = T_5 \begin{bmatrix} u_{m,i} \\ u_{b,j} \end{bmatrix} \tag{28}$$

The Condensed Craig-Bampton transformation can be obtained from the global assembly as:

$$u \simeq T_{CB} T_5 \begin{bmatrix} u_{m,i} \\ u_{b,j} \end{bmatrix} = T_{CCB} \begin{bmatrix} u_{m,i} \\ u_{b,j} \end{bmatrix} \tag{29}$$

and transforming the equation of motion onto the Condensed Craig-Bampton reduction basis:

$$M_{CCB} \begin{bmatrix} \ddot{u}_{m,i} \\ \ddot{u}_{b,j} \end{bmatrix} + K_{CCB} \begin{bmatrix} u_{m,i} \\ u_{b,j} \end{bmatrix} = T_{CCB}^T f \tag{30}$$

Results in a reduced equation of motion, derived from the Craig-Bampton equation of motion (24) by condensing the *retained* interface displacements $u_{b,k}$.

4.1.3. Free-interface primal Component Mode Synthesis methods

Free-interface methods are another subcategory of CMS. In these types of methods, the substructures are approximated by a truncated set of their modes and connected to each other by attachment modes. Unlike fixed-interface methods, these do not require an initial separation of the components DOF into internal and interface. In this subsection we study these methods in a primal assembly formulation, which requires a slightly different approach than fixed-interface methods.

Rubin's method. The Rubin Method [20] approximates the displacement of each component s using a truncated set of modes. These modes contain all displacement DOF, not only the internal ones as in the Craig-Bampton Method (20).

$$u \simeq \begin{bmatrix} \Phi & G_r B_{bb}^T \end{bmatrix} \begin{bmatrix} u_m \\ g_b \end{bmatrix} = T_6 \begin{bmatrix} u_m \\ g_b \end{bmatrix} \tag{31}$$

With g_b being the interface subset of the interface force vector g in the equation of motion (2), Φ the block diagonal matrix containing the truncated set of modes of all N substructures, G_r the block-diagonal matrix containing the residual flexibility matrices of each component, B_{bb} the matrix that selects the interface DOF from the global set (as defined in (8)), and u_m the block-vector of modal participation factors related to all components.

The residual flexibility matrix G_r can be obtained by subtracting the retained modes from the flexibility matrix K^{-1}:

$$G_r = K^{-1} - \Phi \Omega^{-2} \Phi^T \tag{32}$$

with K^{-1} a block-diagonal matrix containing the inverses of each component stiffness matrix (also referred to as component flexibilities) and Ω^{-2} the diagonal matrix containing the inverses of the first eigenvalues of each component. If the stiffness matrix K is singular due to insufficient boundary conditions to restrict its rigid body motion, then K^{-1} is computed using a procedure that enforces invertibility while eliminating the rigid body modes as explained in [3].

The Eq. (31) can be multiplied by B_{bb} on the left to obtain the uncoupled interface displacements. The transformation to get the modal participation factors and the uncoupled interface displacements results in:

$$u_{b,0} = B_{bb}u \simeq \begin{bmatrix} B_{bb}\Phi & B_{bb}G_r B_{bb}^T \end{bmatrix} \begin{bmatrix} u_m \\ g_b \end{bmatrix} = \begin{bmatrix} \Phi_b & G_{r,bb} \end{bmatrix} \begin{bmatrix} u_m \\ g_b \end{bmatrix} \tag{33}$$

From the previous transformation, the interface forces g_b can be expressed in terms of u_m and $u_{b,0}$ by inverting the interface residual flexibility matrix $G_{r,bb}$. The modal participation factors u_m and the interface forces g_b can be obtained as:

$$\begin{bmatrix} u_m \\ g_b \end{bmatrix} = \begin{bmatrix} I & 0 \\ -G_{r,bb}^{-1}\Phi_b & G_{r,bb}^{-1} \end{bmatrix} \begin{bmatrix} u_m \\ u_{b,0} \end{bmatrix} = \begin{bmatrix} I & 0 \\ -K_{r,bb}\Phi_b & K_{r,bb} \end{bmatrix} \begin{bmatrix} u_m \\ u_{b,0} \end{bmatrix} = T_7 \begin{bmatrix} u_m \\ u_{b,0} \end{bmatrix} \tag{34}$$

Up to this point, neither equilibrium nor compatibility have been established yet. In the primal assembly, a common set of interface displacements u_b is used, which establishes compatibility and equilibrium at the same time. The Rubin Method is thus primally assembled similarly as done in Eq. (9).

$$\begin{bmatrix} u_m \\ u_{b,0} \end{bmatrix} = \begin{bmatrix} I & 0 \\ 0 & A_{bb}^T \end{bmatrix} \begin{bmatrix} u_m \\ u_b \end{bmatrix} = T_8 \begin{bmatrix} u_m \\ u_b \end{bmatrix} \tag{35}$$

Finally, the division of u_b in *retained* and *prescribed* interface terms can be done similarly as in Eq. (11):

$$\begin{bmatrix} u_m \\ u_b \end{bmatrix} = \begin{bmatrix} I & 0 & 0 \\ 0 & B_{b,k} & B_{b,j} \end{bmatrix} \begin{bmatrix} u_m \\ u_{b,k} \\ u_{b,j} \end{bmatrix} = T_9 \begin{bmatrix} u_m \\ u_{b,k} \\ u_{b,j} \end{bmatrix} \tag{36}$$

The Rubin transformation can be thus obtained by concatenation of the previous transformations:

$$u \simeq T_6 T_7 T_8 T_9 \begin{bmatrix} u_m \\ u_{b,k} \\ u_{b,j} \end{bmatrix} = T_R \begin{bmatrix} u_m \\ u_{b,k} \\ u_{b,j} \end{bmatrix} \tag{37}$$

And as done in previous methods, the equation of motion is projected onto the Rubin reduction basis:

$$M_R \begin{bmatrix} \ddot{u}_m \\ \ddot{u}_{b,k} \\ \ddot{u}_{b,j} \end{bmatrix} + K_R \begin{bmatrix} u_m \\ u_{b,k} \\ u_{b,j} \end{bmatrix} = T_R^T f \tag{38}$$

Where the matrices M_R and K_R are obtained as:

$$M_R = \begin{bmatrix} M_{mm} & M_{mk} & M_{mj} \\ M_{km} & M_{kk} & M_{kj} \\ M_{jm} & M_{jk} & M_{jj} \end{bmatrix} = T_R^T M T_R, \quad K_R = \begin{bmatrix} K_{mm} & K_{mk} & K_{mj} \\ K_{km} & K_{kk} & K_{kj} \\ K_{jm} & K_{jk} & K_{jj} \end{bmatrix} = T_R^T K T_R \tag{39}$$

Similarly to the Craig-Bampton equation of motion (24), both equilibrium and compatibility conditions are inherently satisfied. It is a reduced system of equations because the number of DOF is reduced with respect to the primal assembly.

MacNeal's method. The MacNeal's Method [17] is a simplification of the Rubin Method, in which the interface inertias are neglected. This process of condensation is similar to that presented in the Condensed Craig-Bampton Method. Consider the *retained* interface terms (second line) of the equation of motion of the Rubin method (38):

$$M_{km}\ddot{u}_m + M_{kk}\ddot{u}_{b,k} + M_{kj}\ddot{u}_{b,j} + K_{km}u_m + K_{kk}u_{b,k} + K_{kj}u_{b,j} = f_{b,k} \tag{40}$$

Assuming that no external forces are being applied, and that the inertial terms are neglegible respect to the stiffness terms:

$$M_{km}\ddot{u}_m \approx 0, \quad M_{kk}\ddot{u}_{b,k} \approx 0, \quad M_{kj}\ddot{u}_{b,j} \approx 0, \quad f_{b,k} = 0 \tag{41}$$

The vector of *retained* interface displacements $u_{b,k}$ can be expressed as a combination of u_m and $u_{b,j}$, in a similar manner as it was done in the Condensed Craig-Bampton Method (27):

$$u_{b,k} \simeq -K_{kk}^{-1} \begin{bmatrix} K_{km} & K_{kj} \end{bmatrix} \begin{bmatrix} u_m \\ u_{b,j} \end{bmatrix} = \begin{bmatrix} \Pi_{km} & \Pi_{kj} \end{bmatrix} \begin{bmatrix} u_m \\ u_{b,j} \end{bmatrix} \tag{42}$$

With this approximation, the Rubin's DOF can be expressed by a reduced set of DOF:

$$\begin{bmatrix} u_m \\ u_{b,k} \\ u_{b,j} \end{bmatrix} \simeq \begin{bmatrix} I & 0 \\ \Pi_{km} & \Pi_{kj} \\ 0 & I \end{bmatrix} \begin{bmatrix} u_m \\ u_{b,j} \end{bmatrix} = T_{10} \begin{bmatrix} u_m \\ u_{b,j} \end{bmatrix} \tag{43}$$

The MacNeal's transformation can be thus obtained by application of transformation T_{10} to the Rubin transformation matrix:

$$u \simeq T_R T_{10} \begin{bmatrix} u_m \\ u_{b,j} \end{bmatrix} = T_{MN} \begin{bmatrix} u_m \\ u_{b,j} \end{bmatrix} \tag{44}$$

The equation of motion is projected onto the MacNeal's reduction basis:

$$M_{MN} \begin{bmatrix} \ddot{u}_m \\ \ddot{u}_{b,j} \end{bmatrix} + K_{MN} \begin{bmatrix} u_m \\ u_{b,j} \end{bmatrix} = T_{MN}^T f \tag{45}$$

This equation of motion condenses out the *retained* interface DOF, thus reducing the size of the equation of motion with respect to the Rubin's method.

4.2. Dual assembly

The dual assembly approach in Dynamic Substructuring refers to a formulation where the system is assembled in a manner such that the interface forces are kept as unknowns. Unlike the primal approach, which intrinsically imposes displacement continuity at substructure interfaces, the dual approach intrinsically imposes force equilibrium across interfaces. This approach involves choosing interface forces of the type

$$g = -B^T \lambda \tag{46}$$

that impose the interface forces to be defined by a unique set of force intensities, which are defined by λ. This set of interface intensities can be interpreted as the Lagrange multipliers (LM) [2]. This definition of the interface forces automatically satisfies the equilibrium condition (4), since it was shown in Eq. (10) that L is the nullspace of B, which means that B^T is the nullspace of L^T.

By inserting the transformation (46), the dynamic substructuring statement (7) can be simplified by suppressing the equilibrium equation, which is inherently satisfied. In block-diagonal format, the system of equations results:

$$\begin{bmatrix} M & 0 \\ 0 & 0 \end{bmatrix} \begin{bmatrix} \ddot{u} \\ \ddot{\lambda} \end{bmatrix} + \begin{bmatrix} K & B^T \\ B & 0 \end{bmatrix} \begin{bmatrix} u \\ \lambda \end{bmatrix} = \begin{bmatrix} f \\ 0 \end{bmatrix} \tag{47}$$

This system of equations is equivalent to the primal assembly (13), since no simplification is done. Analogously as explained in Section 4.1, the LM can be split in *retained* and *prescribed*, as λ_k and λ_j, respectively. This differentiation is equivalent as in the primal assembly: the *retained* DOF correspond to interfaces that lay within the passive assembly, whereas the *prescribed* DOF are related to the active-passive interfaces. This separation is also done by using the matrices $B_{b,k}$ and $B_{b,j}$ as defined in Eq. (11).

$$\begin{bmatrix} u \\ \lambda \end{bmatrix} = \begin{bmatrix} I & 0 & 0 \\ 0 & B_{b,k} & B_{b,j} \end{bmatrix} \begin{bmatrix} u \\ \lambda_k \\ \lambda_j \end{bmatrix} = T_d \begin{bmatrix} u \\ \lambda_k \\ \lambda_j \end{bmatrix} \tag{48}$$

The dual assembly equation of motion (47) can be thus projected using T_d to separate the *retained* and *prescribed* terms:

$$M_d \begin{bmatrix} \ddot{u} \\ \ddot{\lambda}_k \\ \ddot{\lambda}_j \end{bmatrix} + K_d \begin{bmatrix} u \\ \lambda_k \\ \lambda_j \end{bmatrix} = T_d^T \begin{bmatrix} f \\ 0 \end{bmatrix} \tag{49}$$

The equation of motion in dual assembly is in the same physical condition as the primal assembly Eq. (13). Solving it requires high demand

for computational resources, and it is sometimes referred to as the *direct solution* or *full solution*.

4.2.1. Dual free-interface Component Mode Synthesis methods

Component Mode Synthesis can also be applied in the dual assembly context. In this subsection, free-interface CMS methods will be introduced first, since they are present in the bibliography. The main CMS method in dual representation is the Dual Craig-Bampton Method [18]. A less expensive method was introduced in the Condensed Dual-Craig Bampton Method [7], which incorporates the simplifications from MacNeal's method into the Dual Craig-Bampton Method.

Dual Craig-Bampton method (DCBM). The DCBM [18] is a CMS method that uses free-interface modes and attachment modes. It contains the same ingredients as the Rubin Method. The displacements are approximated as in Eq. (31). In this case, instead of representing g in terms of g_b, it is done by the Lagrange multipliers, resulting in the following transformation:

$$\begin{bmatrix} u \\ \lambda_k \\ \lambda_j \end{bmatrix} \simeq \begin{bmatrix} \Phi & -G_r B^T B_{b,k} & -G_r B^T B_{b,j} \\ 0 & I & 0 \\ 0 & 0 & I \end{bmatrix} \begin{bmatrix} u_m \\ \lambda_k \\ \lambda_j \end{bmatrix} = T_{11} \begin{bmatrix} u_m \\ \lambda_k \\ \lambda_j \end{bmatrix} \tag{50}$$

The DCBM transformation can be thus obtained by concatenation of the previous transformation to the dual transformation (48):

$$\begin{bmatrix} u \\ \lambda \end{bmatrix} \simeq T_d T_{11} \begin{bmatrix} u_m \\ \lambda_k \\ \lambda_j \end{bmatrix} = T_{DCB} \begin{bmatrix} u_m \\ \lambda_k \\ \lambda_j \end{bmatrix} \tag{51}$$

The dual equation of motion can be projected in the DCBM subspace, as done in previous methods:

$$M_{DCB} \begin{bmatrix} \ddot{u}_m \\ \ddot{\lambda}_k \\ \ddot{\lambda}_j \end{bmatrix} + K_{DCB} \begin{bmatrix} u_m \\ \lambda_k \\ \lambda_j \end{bmatrix} = T_{DCB}^T \begin{bmatrix} f \\ 0 \end{bmatrix} \tag{52}$$

Where the matrices M_{DCB} and K_{DCB} are obtained as:

$$M_{DCB} = \begin{bmatrix} M_{mm} & M_{mk} & M_{mj} \\ M_{km} & M_{kk} & M_{kj} \\ M_{jm} & M_{jk} & M_{jj} \end{bmatrix} = T_{DCB}^T M T_{DCB},$$
$$K_{DCB} = \begin{bmatrix} K_{mm} & K_{mk} & K_{mj} \\ K_{km} & K_{kk} & K_{kj} \\ K_{jm} & K_{jk} & K_{jj} \end{bmatrix} = T_{DCB}^T K T_{DCB} \tag{53}$$

Condensed dual Craig-Bampton method (CDCBM). This method is presented by the authors of this paper in [7]. It starts from the DCBM but with the application of the simplifications of MacNeal's method (41) in the dual approach, which involve that the terms of the equation of motion of the DCBM (52) can be simplified as:

$$M_{km}\ddot{u}_m \approx 0, \quad M_{kk}\ddot{\lambda}_k \approx 0, \quad M_{kj}\ddot{\lambda}_j \approx 0, \quad f_{b,k} = 0 \tag{54}$$

These approximations lead to λ_k to be expressed as a combination of u_m and λ_j:

$$\lambda_k \simeq -K_{kk}^{-1} \begin{bmatrix} K_{km} & K_{kj} \end{bmatrix} \begin{bmatrix} u_m \\ \lambda_j \end{bmatrix} = \begin{bmatrix} \Psi_{km} & \Psi_{kj} \end{bmatrix} \begin{bmatrix} u_m \\ \lambda_j \end{bmatrix} \tag{55}$$

With this approximation, the DCBM DOF can be expressed by a reduced set:

$$\begin{bmatrix} u_m \\ \lambda_k \\ \lambda_j \end{bmatrix} \simeq \begin{bmatrix} I & 0 \\ \Psi_{km} & \Psi_{kj} \\ 0 & I \end{bmatrix} \begin{bmatrix} u_m \\ \lambda_j \end{bmatrix} = T_{12} \begin{bmatrix} u_m \\ \lambda_j \end{bmatrix} \tag{56}$$

The CDCBM transformation can be thus obtained by application of transformation T_{12} in combination with the T_{DCB}:

$$\begin{bmatrix} u \\ \lambda \end{bmatrix} \simeq T_{DCB} T_{12} \begin{bmatrix} u_m \\ \lambda_j \end{bmatrix} = T_{CDCB} \begin{bmatrix} u_m \\ \lambda_j \end{bmatrix} \tag{57}$$

The equation of motion is projected onto the CDCBM reduction basis:

$$M_{CDCB} \begin{bmatrix} \ddot{u}_m \\ \ddot{\lambda}_j \end{bmatrix} + K_{CDCB} \begin{bmatrix} u_m \\ \lambda_j \end{bmatrix} = T_{CDCB}^T \begin{bmatrix} f \\ 0 \end{bmatrix} \tag{58}$$

This equation of motion condenses out the *retained* interface DOF, as done in MacNeal's method, thus reducing the size of the equation of motion with respect to the DCBM.

4.2.2. Fixed dual Craig-Bampton method (FDCBM)

This section introduces a new dual CMS method. It is strictly derived from the Craig-Bampton method. Unlike the DCBM, this new method uses a Craig-Bampton transformation, meaning that it utilizes internal modes and constraint modes. For that, it is necessary to divide the displacement vector into internal and interface uncoupled DOF as in Eq. (8). The transformation of the dual DOF from the dual assembly (48) is:

$$\begin{bmatrix} u \\ \lambda_k \\ \lambda_j \end{bmatrix} = \begin{bmatrix} B_{ii}^T & B_{bb}^T & 0 & 0 \\ 0 & 0 & I & 0 \\ 0 & 0 & 0 & I \end{bmatrix} \begin{bmatrix} u_i \\ u_{b,0} \\ \lambda_k \\ \lambda_j \end{bmatrix} = T_{13} \begin{bmatrix} u_i \\ u_{b,0} \\ \lambda_k \\ \lambda_j \end{bmatrix} \tag{59}$$

Introducing the CBM transformation, the internal displacements can be approximated by internal modes and constraint modes:

$$\begin{bmatrix} u_i \\ u_{b,0} \\ \lambda_k \\ \lambda_j \end{bmatrix} \simeq \begin{bmatrix} \Phi_i & \Psi_{ib,0} & 0 & 0 \\ 0 & I & 0 & 0 \\ 0 & 0 & I & 0 \\ 0 & 0 & 0 & I \end{bmatrix} \begin{bmatrix} u_{m,i} \\ u_{b,0} \\ \lambda_k \\ \lambda_j \end{bmatrix} = T_{14} \begin{bmatrix} u_{m,i} \\ u_{b,0} \\ \lambda_k \\ \lambda_j \end{bmatrix} \tag{60}$$

where $\Psi_{ib,0}$ is obtained as:

$$\Psi_{ib,0} = -K_{ii}^{-1} K_{ib,0}, \quad K_{ib,0} = B_{ii} K B_{bb} \tag{61}$$

In the Craig-Bampton method, K_{ib} implicitly includes the compatibility condition, whereas in this method compatibility is enforced using the compatibility equation explicitly. Otherwise, the interface forces cannot be accessed because of the intrinsic satisfaction of the equilibrium condition inherent to the primal assembly. The FDCBM transformation can be thus obtained by concatenation of the previous transformations to the dual transformation (48):

$$\begin{bmatrix} u \\ \lambda \end{bmatrix} \simeq T_d T_{13} T_{14} \begin{bmatrix} u_{m,i} \\ u_{b,0} \\ \lambda_k \\ \lambda_j \end{bmatrix} = T_{FDCB} \begin{bmatrix} u_{m,i} \\ u_{b,0} \\ \lambda_k \\ \lambda_j \end{bmatrix} \tag{62}$$

The dual equation of motion can be projected in the FDCBM subspace:

$$M_{FDCB} \begin{bmatrix} \ddot{u}_{m,i} \\ \ddot{u}_{b,0} \\ \ddot{\lambda}_k \\ \ddot{\lambda}_j \end{bmatrix} + K_{FDCB} \begin{bmatrix} u_{m,i} \\ u_{b,0} \\ \lambda_k \\ \lambda_j \end{bmatrix} = T_{FDCB}^T \begin{bmatrix} f \\ 0 \end{bmatrix} \tag{63}$$

This new approach offers some advantages over the Craig-Bampton Method and the Dual Craig-Bampton Method:

- The Craig-Bampton Method does not explicitly provide interface forces, whereas the Fixed Dual Craig-Bampton Method enables their direct computation. This is advantageous for enforcing force-based Numerical Transfer Path Analysis.
- The Dual Craig-Bampton Method introduces modal reduction and correction terms that modify interface displacements, leading to an incomplete enforcement of the compatibility condition. In contrast, FDCBM preserves interface displacement degrees of freedom in their physical representation, ensuring full compatibility between subdomains.

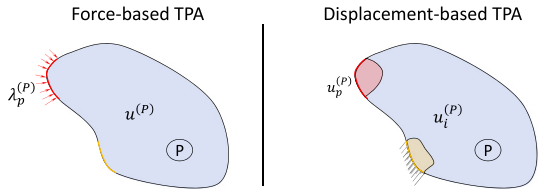

Fig. 6. Force-based and displacement-based transfer path analysis paradigm.

5. Imposing prescribed conditions

In the previous sections, the primal and dual methods were derived by distinguishing between the interface degrees of freedom that are retained $u_{b,k}, \lambda_k$ and those that are prescribed $u_{b,j}, \lambda_j$. This classification is essential for applying Transfer Path Analysis using Dynamic Substructuring, as it determines whether force-based or displacement-based boundary conditions are imposed.

Two families of TPA can be analyzed from this perspective, as seen in Fig. 6:

- **Force-based TPA (f-TPA)**. Dual methods impose interface forces at the active-passive interfaces. For each active-passive interface contained in λ_j, a prescribed load λ_p is established. The remaining active-passive interfaces contain no boundary conditions.
- **Displacement-based TPA (u-TPA)**. Primal methods impose interface displacements at the *prescribed* active-passive interfaces. The non-prescribed active-passive interfaces are fixed. This condition is a fixed-interface condition.

In both families, the prescribed subset of interface DOF needs to be explicitly enforced in the equation of motion. To implement these conditions within the DS approach, the mass and stiffness (and given the case, the damping) matrices in the equation of motion need to be modified.

To achieve that in the displacement-based TPA framework, take the primal equation of motion of subsystem P_i (13), as an example for the procedure, and impose the prescribed displacement condition as:

$$\begin{bmatrix} M_{ii} & M_{ik} & M_{ij} \\ M_{ki} & M_{kk} & M_{kj} \\ 0 & 0 & 0 \end{bmatrix} \begin{bmatrix} \ddot{u}_i \\ \ddot{u}_{b,k} \\ \ddot{u}_{b,j} \end{bmatrix} + \begin{bmatrix} K_{ii} & K_{ik} & K_{ij} \\ K_{ki} & K_{kk} & K_{kj} \\ 0 & 0 & I \end{bmatrix} \begin{bmatrix} u_i \\ u_{b,k} \\ u_{b,j} \end{bmatrix} = \begin{bmatrix} 0 \\ 0 \\ u_p \end{bmatrix} \tag{64}$$

with u_p the prescribed displacement vector. Here, the terms of the mass and stiffness matrices M_{pr}, K_{pr} corresponding to the prescribed DOF are converted to zero, and K_{jj} is replaced with the identity matrix to enforce the equality $u_{b,j} = u_p$. The exact same procedure can be applied to all the Dynamic Substructuring and Component Mode Synthesis methods presented in the previous sections and shown in Table 2. In the case of dual methods, the imposed equality is $\lambda_j = \lambda_p$.

The vector u_p is populated by zeros at the non-prescribed active-passive interfaces, and non-zeros at the prescribed part. These non-zero terms correspond to the active-passive displacement DOF obtained from the analysis of the assembly AP. In the case of primal methods, this means that the non-prescribed active-passive interfaces are fixed. When dual methods are used, for the prescribing vector λ_p the same rule applies, and it has the physical meaning of removing any boundary conditions at non-prescribed active-passive interfaces. The Fig. 6 illustrates this differentiation.

The solution of the *prescribed* system of Eq. (64) and its equivalent formulations for other methods determines the displacement field and interface degrees of freedom at the studied interface j within the passive level P_i. This hierarchical process, illustrated in Fig. 7, enables a structured evaluation of the response propagation through successive subsystem levels.

At each hierarchical level, the total response is obtained by summing the contributions from all transfer paths. The aggregated response at level P_i must be equivalent to the response of the subset P_i within the original assembly AP at the initial level:

$$u_T^{(P_i)} = \sum_{j=1}^{n_{\text{paths}}} u_j^{(P_i)} \rightarrow u_{AP}^{(P_i)} \tag{65}$$

where $u_T^{(P_i)}$ represents the total displacement field at the i-th level of the passive subsystem P_i, $u_j^{(P_i)}$ denotes the displacement field of P_i resulting from the imposed condition at interface j, and $u_{AP}^{(P_i)}$ corresponds to the response of the original assembly AP within the subset P_i. The arrow indicates that the first term should tend to the second, which in the physical representation (primal and dual methods) is achieved, but when Component Mode Synthesis is applied some uncertainties may accumulate throughout the TPA levels.

6. Validation

In this section, the novel simulation-based Transfer Path Analysis methodology is validated by comparing its transfer-path contributions against those obtained from an analytical mass–spring model, inspired by the validation example found in [14]. The system is partitioned into TPA sublevels, as illustrated in Fig. 8(a), where the six connection interfaces are also indicated. The novel TPA formulation is applied using the dual assembly, which enables the explicit computation of interface forces and their imposition at each sublevel.

The corresponding Finite Element model is shown in Fig. 8(b), where the division of the system into five substructures for the dynamic-substructuring framework is depicted. Each substructure consists of a shell plate representing a lumped mass and several shell-element strips representing the springs. The plate material is assigned an artificially high Young's modulus to enforce near-rigid behavior, while the spring strips use a low-density material so that their mass is negligible. The spring constants of the analytical model are reproduced numerically by selecting a rectangular section of area $A = 1\ \text{mm}^2$ and assigning a Young's modulus of $E = 2$ GPa to the spring strips. Similarly, the physical masses of the rigid plates are matched by enforcing a density of $\rho = 7850\ \text{kg/m}^3$. All rotational and translational degrees of freedom are fixed, except in the global X direction, ensuring that the system behaves as a one-dimensional mass–spring chain.

The analytical TPA begins by constructing the global stiffness and mass matrices of the full assembly and solving the harmonic equilibrium equation

$$-\omega^2 M_{an}^{(AP)} u_{an}^{(AP)} + K_{an}^{(AP)} u_{an}^{(AP)} = f_{an}^{(AP)}, \tag{66}$$

where $M_{an}^{(AP)} = \text{diag}(m_1, m_2, \dots, m_5)$, $f_{an}^{(AP)} = [f_1, 0, 0, 0, 0]^T$, and $K_{an}^{(AP)}$ is given by

$$K_{an}^{(AP)} = \begin{bmatrix} k_{12}+k_{13} & -k_{12} & -k_{13} & 0 & 0 \\ -k_{12} & k_{12}+k_{23}+k_{24} & -k_{23} & -k_{24} & 0 \\ -k_{13} & -k_{23} & k_{13}+k_{23}+k_{35} & 0 & -k_{35} \\ 0 & -k_{24} & 0 & k_{24}+k_{45} & -k_{45} \\ 0 & 0 & -k_{35} & -k_{45} & k_{35}+k_{45} \end{bmatrix}. \tag{67}$$

At subsequent TPA sublevels, the displacements obtained at level AP are used to compute the effective interface forces. At sublevel P_2, for instance, interfaces 2, 3, and 4 become active, associated respectively with the elastic forces induced by springs k_{13}, k_{24}, and k_{23}. The interface forces are therefore

$$g_2^{(P_2)} = k_{13}(x_1^{(AP)} - x_3^{(AP)}), \qquad g_3^{(P_2)} = k_{24}(x_2^{(AP)} - x_4^{(AP)}), \qquad g_4^{(P_2)} = k_{23}(x_2^{(AP)} - x_3^{(AP)}). \tag{68}$$

Each of these forces is applied independently to the corresponding reduced sublevel system, which is solved through

$$-\omega^2 M_{an}^{(P_2)} u_i^{(P_2)} + K_{an}^{(P_2)} u_i^{(P_2)} = g_i^{(P_2)}, \tag{69}$$

where the subscript i identifies the individual path contribution under evaluation.

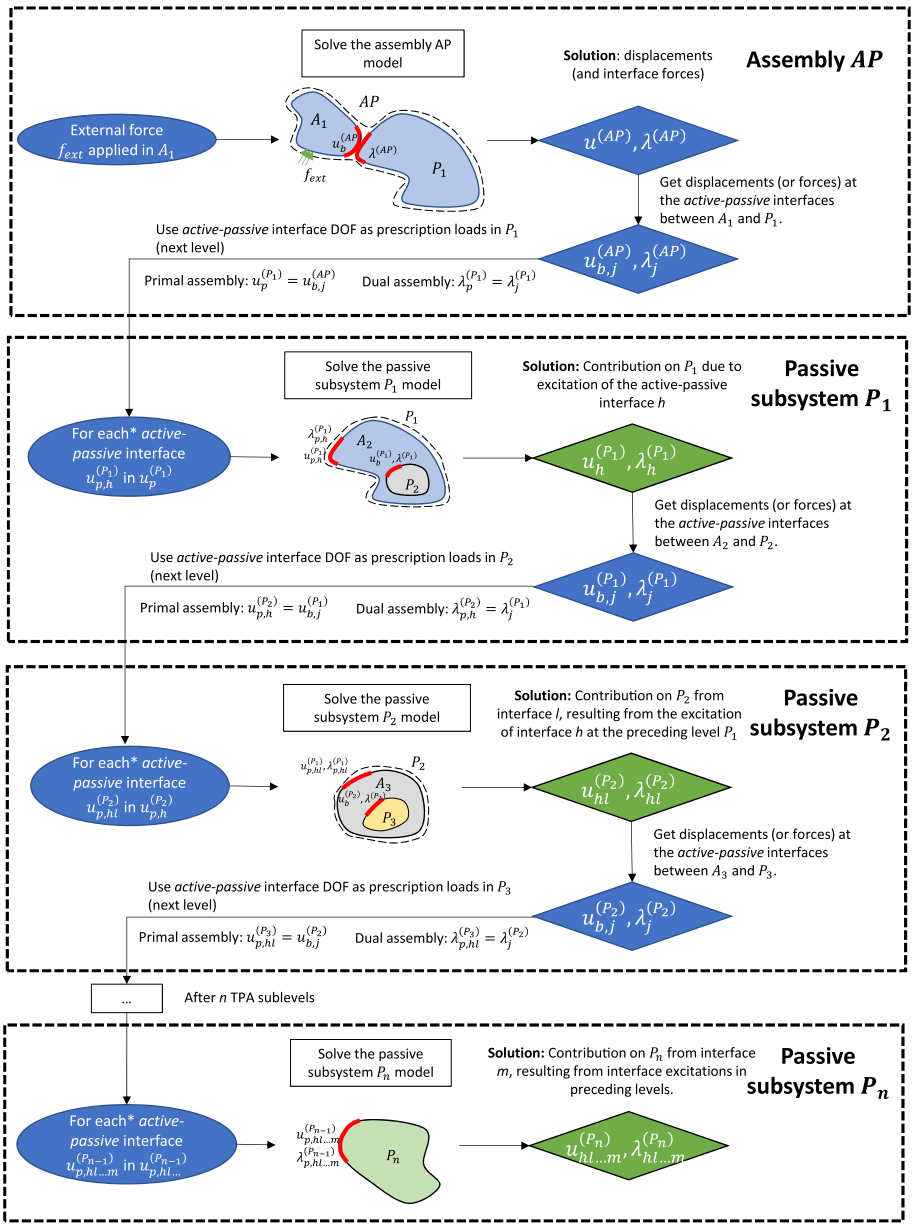

Fig. 7. Multilevel transfer path analysis workflow. At each level, every active-passive interface set contains different contact interfaces, which are the different transfer paths between active and passive components.

A comparison between the analytical contributions and those computed using the FE-based novel TPA methodology with a dual approach is presented in Fig. 9. Results for sublevels P_2 and P_3 are shown in Fig. 9(a) and (b), respectively. The behavior of both models is almost identical. This agreement is quantified in Fig. 9(c), which displays the absolute relative error between analytical and FE-based contributions. The errors remain below 0.1%, demonstrating that the novel TPA formulation accurately reproduces the analytical transfer-path contributions.

7. Example

To demonstrate the applicability and performance of the presented framework, a numerical example based on a simplified two-story building structure is presented, as shown in Fig. 10. The model is subdivided into multiple substructures (see Fig. 11), discretized using linear shell elements. The division of the domain by substructures allows grouping them into the different TPA levels, as presented in Table 3. The material used in this example is isotropic concrete, with density ρ = 2392 kg/m^3, Young's Modulus E = 19.36 GPa and Poisson's Ratio ν = 0.1414. The thickness of the Finite Element shells is t_{wall} = 0.5 m, t_{floor} = 0.6 m, t_{ceil} = 0.4 m, corresponding to the substructures as described in Fig. 10.

A low-frequency excitation is applied at the assembly level AP, considered the level zero of the multilevel TPA framework. The load is introduced specifically in subdomain s_1, as illustrated in Fig. 10. At each subsequent TPA level, different interfaces are analyzed as transmission paths. In level AP, all subdomains are assembled together. At level P_1, the interface displacements (or forces) resulting from the excitation in AP are analyzed through paths 1, 2, 3, and 4, which constitute the active-passive interfaces. The interface displacements (or forces) obtained at this level serve as inputs for level P_2, where the transmission is studied across interfaces 5 and 6. Finally, in level P_3, the propagation continues through interfaces 5, 7, and 8, completing the hierarchical evaluation of the transfer paths.

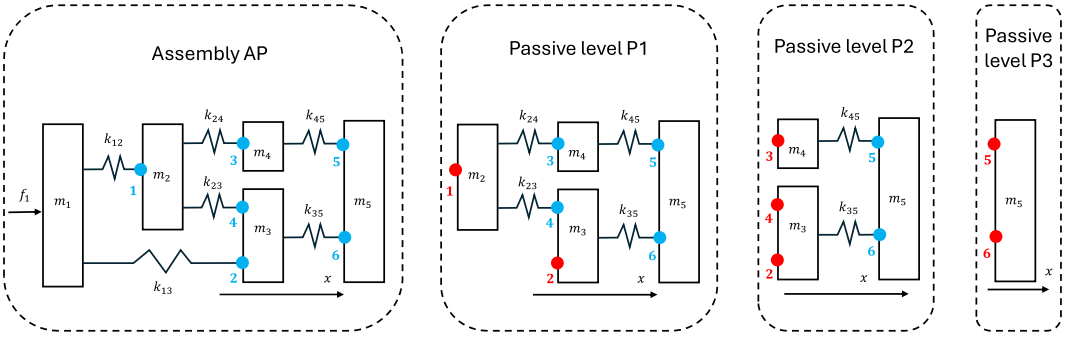

(a) Analytical mass-spring system diagram.

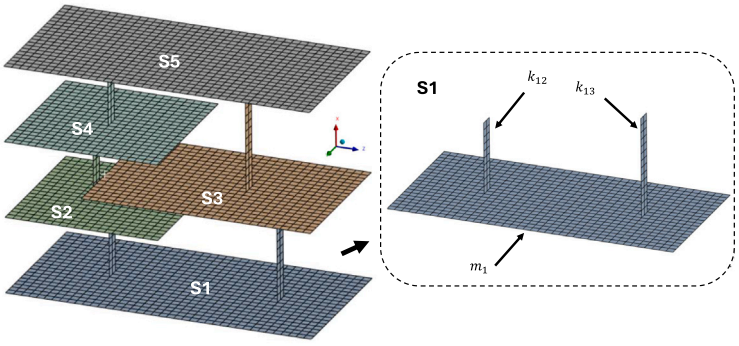

(b) Finite Element model of the mass-spring system.

Fig. 8. Analytical and FE model of the mass-spring system.

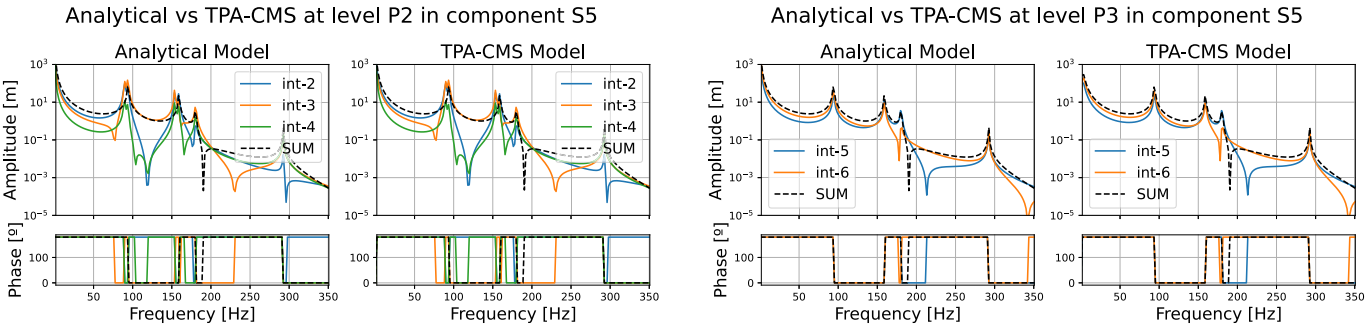

(a) Contributions at level P2 in component S5.

(b) Contributions at level P3 in component S5.

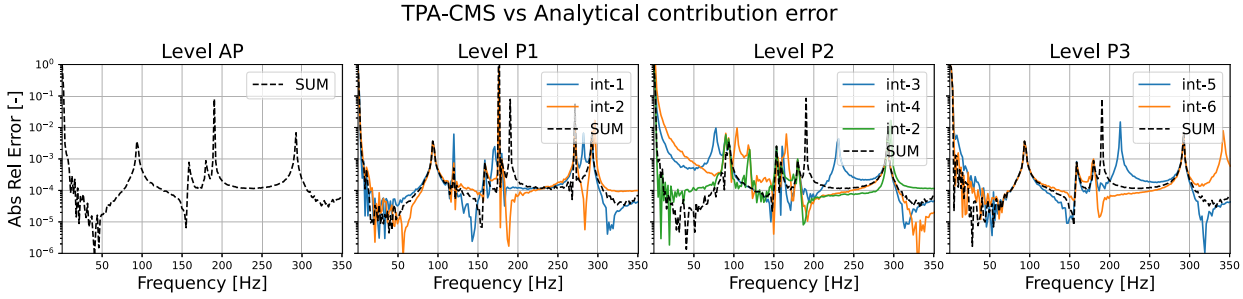

(c) Contribution errors, CMS-TPA vs Analytical, at different TPA levels on the validation model in component S5.

Fig. 9. Analytical vs TPA-CMS contribution results on the validation model.

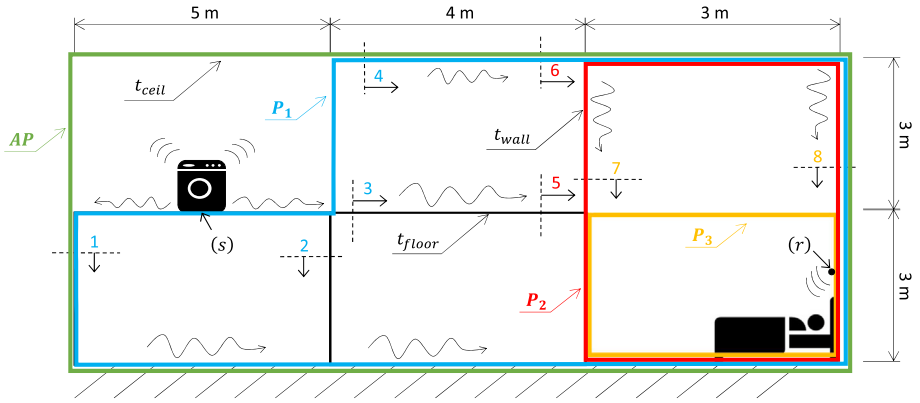

Fig. 10. Example used for transfer path analysis using dynamic substructuring. The different TPA levels are highlighted in green (AP), blue (P_1), red (P_2) and yellow (P_3).

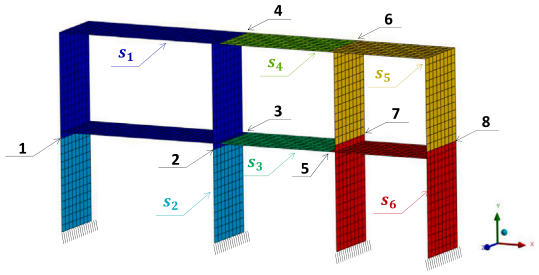

Fig. 11. Finite element model and subdivision of the domain.

Table 3
Levels of the multilevel transfer path analysis. Each level contains a set of subdomains defined in the dynamic substructuring decomposition. The studied interfaces act as external loads to the level.

Level	Domains	Studied interfaces
AP	s_1, s_2, s_3, s_4, s_5, s_6	–
P_1	s_2, s_3, s_4, s_5, s_6	1, 2, 3, 4
P_2	s_5, s_6	5, 6
P_3	s_6	5, 7, 8

The objective of this example is to trace the different transmission paths from the source location (s) to the receiver (r), and to identify which paths contribute most significantly to the overall dynamic response. The analysis is structured in two main parts. The first part focuses on evaluating the accuracy and computational efficiency of CMS methods for Numerical TPA. Each method is assessed by comparing its results with those obtained from the full physical model. This part also investigates how errors propagate through the multilevel hierarchy of the Transfer Path Analysis, offering insight into how inaccuracies may accumulate with each additional TPA level. Additionally, the computational performance of each CMS method is analyzed in terms of CPU time and memory (RAM) consumption, allowing for a balanced evaluation of accuracy versus resource requirements.

The second part explores Transfer Path Analysis using two distinct formulations: displacement-based TPA (u-TPA), which is implemented using a primal CMS method, and force-based TPA (f-TPA), conducted through a dual CMS method. These approaches are compared to exhibit the different contribution results offered by the two methodologies.

7.1. Evaluation of CMS accuracy and efficiency

The methods listed in Table 2 are evaluated in this analysis. All approaches are subjected to the same external load, applied at the source location (s), and their results are compared against the reference solution obtained using the *primal assembly* method at level zero (AP). The comparison is based on the relative error at the receiver location (r), computed using the vector norm as:

$$e_{r,\text{method,rel},\,P_i} = \frac{\left|u_{r,\text{method},\,P_i} - u_{r,\text{primal},\,AP}\right|}{\left|u_{r,\text{primal},\,AP}\right|} \tag{70}$$

For the modal method, the first 100 modes are retained at each TPA sublevel. In the CMS-based approaches, 20 component modes are used in the fixed-interface methods, while 30 modes are employed for the free-interface methods. The mode count for each case is selected based on the highest frequency analyzed (100 Hz), ensuring that the last retained mode corresponds to an eigenfrequency of at least twice this value (200 Hz), providing sufficient resolution across the frequency range of interest.

Fig. 12 uses colored tags to categorize the various methods: physical methods are shown in *green*, the modal method in *yellow*, fixed-interface CMS methods in *blue*, and free-interface CMS methods in *red*. As expected, the physical methods (*primal* and *dual*) yield very low relative errors across the different TPA levels, with deviations attributed to numerical solver inaccuracies. In contrast, the modal method results in errors exceeding 100%, rendering it unsuitable for this analysis. A similar trend is observed for the free-interface CMS methods, which also produce errors above 100% in the frequency range under study. Among the reduced-order approaches, only fixed-interface methods prove to be reliable. Notably, CBM and FDCBM yield nearly identical error levels, indicating that they are functionally equivalent in this context. The CCBM, while computationally efficient, generally shows higher errors compared to the other fixed-interface methods, and its errors propagate throughout different TPA levels. It is also observed that all reduced-order methods, including the fixed-interface approaches, exhibit a decline in accuracy as the excitation frequency increases, which is consistent with the typical limitations of modal truncation.

Fig. 13 presents a comparative analysis of the CPU time, RAM usage, and Median Absolute Relative Error (MARE) for the different methods. The colormap in the figure visually encodes the MARE values, which are calculated as follows:

$$\text{MARE} = \text{median}(e_{r,\text{method,rel},P_3}) \tag{71}$$

Here, $e_{r,\text{method,rel},P_3}$ represents the relative error of each method at the final TPA level P_3, evaluated at the receiver location, as previously defined in Eq. (70). The median is computed across the entire studied frequency range.

The comparison of methods reveals that CMS techniques and the modal method generally require less CPU time than the full primal and

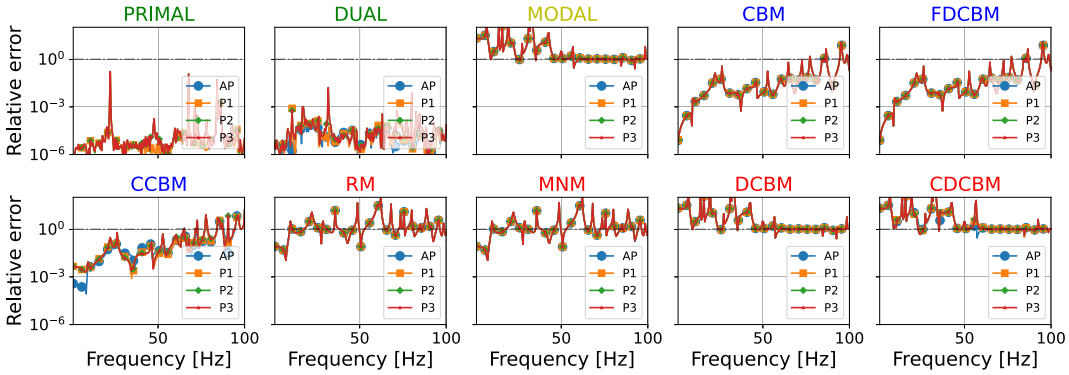

Fig. 12. Propagation of errors within the multilevel TPA example. Errors relative to the primal method at assembly AP level.

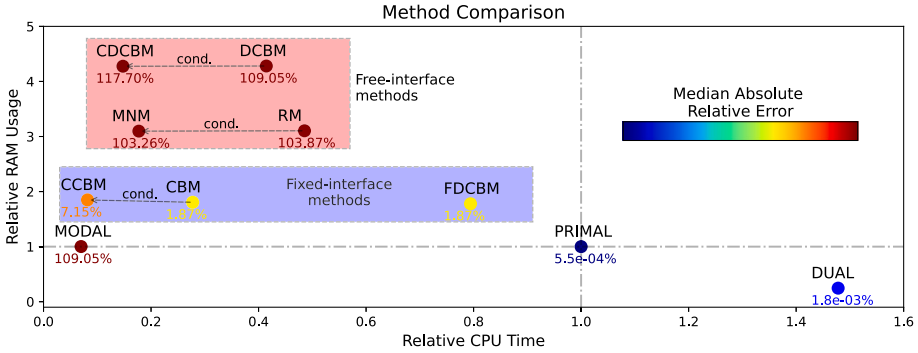

Fig. 13. Comparative of CPU time, RAM usage and median relative error for the different studied methods. The variables are relative to the primal assembly. The different CMS methods are grouped by type, and the condensed methods are connected to their non-condensed counterparts.

dual assemblies. Among the evaluated approaches, free-interface methods (MNM, RM, DCBM, and CDCBM) exhibit both high RAM consumption and high relative error, making them unsuitable for performing accurate numerical TPA.

In contrast, fixed-interface methods (CBM, FDCBM, and CCBM) demonstrate better performance, with lower relative errors and more moderate RAM usage, although RAM demand may still pose limitations in large-scale applications. Notably, condensed methods (CCBM, MNM, and CDCBM) offer a reduction in CPU time compared to their non-condensed counterparts, while maintaining similar RAM requirements.

The FDCBM method requires similar memory as CBM but at the cost of increased CPU time, whereas CCBM provides a favorable trade-off between accuracy and computational efficiency. Regarding the modal method, although it shows the lowest CPU and RAM usage overall, its high error renders it inappropriate for TPA.

It is important to note that these results are specific to the case study presented and may vary depending on the system characteristics and model complexity. However, some general trends can be identified. Free-interface methods tend to consume more RAM and CPU time due to the need to invert larger stiffness matrices, which are typically less efficient to handle compared to those in fixed-interface methods.

Another important consideration is the number of component modes required in each method. Fixed-interface methods offer an additional advantage over free-interface methods in this regard. Due to the boundary constraints imposed at the interfaces, the natural frequencies of fixed-interface substructures are shifted to higher values. As a result, a smaller number of modes is typically sufficient to accurately represent the system dynamics within the frequency range of interest. In contrast, free-interface methods lack such constraints, leading to lower natural frequencies and requiring a greater number of modes to achieve comparable accuracy, further increasing the computational cost.

Additionally, all CMS methods generally demand more memory than the full *primal* and *dual* assemblies, as the inversion of sparse stiffness matrices leads to dense representations [7]. When selecting an appropriate method, it is essential to evaluate the trade-offs between computational cost (RAM and CPU) and solution accuracy. For instance, the CCBM provides very fast preliminary results when memory is not a limiting factor. The CBM offers more accurate results at slightly higher computational cost. The FDCBM is particularly useful when interface force estimation is required. However, for complete and most accurate results, the full *primal* or *dual* assemblies should be employed.

7.2. Evaluation of displacement- and force-based transfer path analyses

In Section 5, two complementary approaches for TPA were introduced: displacement-based TPA (u-TPA), which relies on imposing interface displacements, and force-based TPA (f-TPA), which is based on prescribing interface forces. These approaches align naturally with the primal and dual formulations of Dynamic Substructuring.

As shown in Section 7.1, the non-condensed fixed-interface CMS methods, CBM for the primal formulation, and the FDCBM for the dual formulation, demonstrated a favorable balance between accuracy and computational efficiency. Given their reliability, these two methods are selected for the evaluation of transfer paths in the numerical example.

This section serves two primary purposes. First, it aims to demonstrate the feasibility of conducting multilevel TPA using the Dynamic Substructuring framework. Second, it compares the contribution results offered by a displacement-based TPA formulation with the traditional force-based. For u-TPA, the Craig-Bampton method is used, whereas for f-TPA the novel Fixed Dual Craig-Bampton method is implemented (Fig. 14).

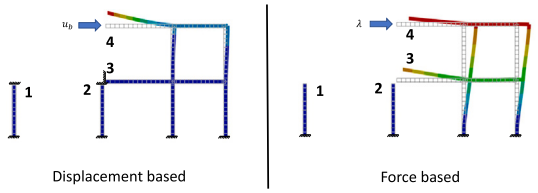

Fig. 14. Description of TPA at level P_1 when prescribing the displacements (left) and forces (right) in interface 4. The displacement-based TPA approach fixes the remaining active-passive interfaces (1, 2, 3) when the interface displacements are prescribed in (4). In the force-based approach, the retained interfaces are fully free, when the force is imposed at the prescribed interface.

Table 4
Comparison of the different path contributions using one-level TPA at 35 Hz. The displacement-based TPA shows that the paths 3, 5 and 8 are the main paths, whereas force-based TPA shows that 4, 6 and 7 are the main ones. Each contribution is relative to the total accumulated constructive contributions.

Level	Path	u-TPA (%)	f-TPA (%)
P1	3	**100**	20.38
	4	−19.96	**79.62**
P2	5	**100**	−65.16
	6	−3.08	**100**
P3	5	18.99	−31.96
	7	7.02	**84.75**
	8	**73.99**	15.25

Table 5
Comparison of the different path contributions using multilevel TPA at 35 Hz. The displacement-based TPA shows that the multilevel path 3-5-8 is the main path, whereas the force-based TPA shows that the multilevel path 4-6-7 is the main one.

Level	Through	Path	u-TPA (%)	f-TPA (%)
P1	–	3	**100**	20.38
		4	−19.96	**79.62**
P2	3	3-5	**99.74**	5.20
		3-6	0.26	1.54
P3	4	4-5	−18.31	−66.96
		4-6	−1.65	**93.27**
	3-5	3-5-5	18.59	13.46
		3-5-7	11.49	−6.25
		3-5-8	**68.38**	−2.48
	3-6	3-6-5	0.00	0.00
		3-6-7	0.51	0.07
		3-6-8	−0.22	1.33
	4-5	4-5-5	−3.59	−27.49
		4-5-7	−3.71	−9.78
		4-5-8	−10.78	−23.84
	4-6	4-6-5	0.00	0.00
		4-6-7	−2.75	**53.41**
		4-6-8	1.02	31.72

7.2.1. One-level TPA vs multilevel TPA

The TPA problem can be approached using either a direct one-level strategy, where displacements or forces obtained from the global level AP are applied directly to a sublevel P_i, or through the multilevel methodology, as described in Section 3. Each approach provides different types of insight: the one-level TPA reveals the direct influence of individual transfer paths from the assembly to each TPA level, while the multilevel TPA captures the cumulative and interactive contributions across intermediate levels.

Both methodologies have been applied in this analysis. To facilitate interpretation, a specific frequency (35 Hz) is first selected for detailed comparison. The results obtained from the one-level and multilevel TPA are summarized in Tables 4 and 5, respectively. Additionally, both displacement-based and force-based formulations are evaluated within each approach.

To assess the influence of individual paths on the overall system response, it is useful to use the concepts of constructive and destructive contributions. Constructive contributions refer to those that increase the magnitude of the total displacement vector, thus aligning in phase and direction. On the other hand, destructive contributions reduce the vector magnitude, indicating phase opposition or partial cancellation between paths.

In the one-level analysis (see Table 4), the u-TPA results indicate that the dominant contributors at each level are 3, 5 and 8 for P_1, P_2, and P_3, respectively. Conversely, the f-TPA results suggest that 4, 6 and 7 are the most significant contributors in the same divisions. These results are consistent with the findings of the multilevel analysis (see Table 5). In the multilevel u-TPA, the multilevel path 3–5–8 emerges as the most influential at level P_3, while the multilevel f-TPA identifies 4–6–7 as the dominant multilevel path.

Both approaches lead to different interpretations: the u-TPA formulation highlights path 3–5–8 as the key contributor, while f-TPA emphasizes path 4–6–7. The multilevel approach provides better insight into how the vibration is transmitted across different assembly levels.

At the selected frequency, the u-TPA method identifies substructure s_3, located between interfaces 3 and 5, as the primary contributor to the overall response. In contrast, the f-TPA approach points to substructure s_4, which lies between interfaces 4 and 6, as the most critical region. However, this observation is frequency-dependent; at other frequencies, different paths dominate the transmission behavior.

In Fig. 15(a) and (b), this phenomenon is observed, where the different contributions vary at distinct excitation frequencies. It is also evident from the different interpretations given by the two methods, u-TPA and f-TPA, as to which are the dominant paths at each excitation frequency.

In the present framework, force-based TPA uses interface forces at the active–passive interfaces as the prescribed quantities. This corresponds directly to force-driven (classical, component-based) TPA, where interface forces act as the primary source and are propagated through the dynamic admittances of the passive side. Such force-driven schemes are regarded as the physically most consistent formulations [22], providing detailed information on source strength, interface loads and structural resonances, and they are therefore the preferred option for accuracy and physical interpretability.

By contrast, displacement-based TPA uses interface displacements prescribed as boundary conditions at selected active–passive interfaces, which is conceptually in line with the transmissibility-based families [22], where path contributions are derived without explicit force reconstruction. According to [22], transmissibility-based methods generally offer easier and faster test setups and are very effective for ranking dominant paths, but they may be less accurate than force-driven methods.

In this context, u-TPA can be viewed as the analogue of transmissibility-based approaches, whereas f-TPA matches the force-driven TPA interpretations. A main drawback of the u-TPA interpretation in the simulation scheme is that the non-prescribed active interfaces must be fixed, which makes a direct comparison with experimental

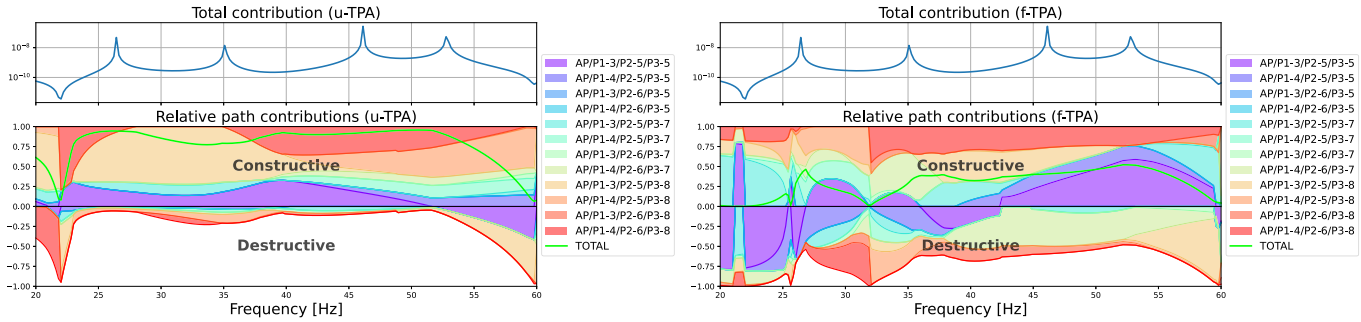

(a) Cumulative u-TPA result. (b) Cumulative f-TPA result

Fig. 15. Cumulative plot of constructive and destructive contributions using u-TPA and f-TPA at sublevel P_3 for the frequency range of 20–60 Hz in a multilevel approach. The contributions are relative to the total accumulated constructive contributions.

transmissibility TPA very impractical: for each interface under analysis, all remaining active interfaces would have to be constrained, adding substantial complexity to the workflow.

8. Conclusions

This work introduces a simulation-based framework for Transfer Path Analysis using Dynamic Substructuring and Component Mode Synthesis. Several CMS methods have been studied and adapted to perform TPA, including Craig-Bampton, Rubin's, MacNeal's and the Dual Craig-Bampton. A novel CMS method, the Fixed-dual Craig-Bampton Method, is presented by combining fixed-interface and constraint modes in a dual assembly formulation. This method, along with the broader framework, facilitates the implementation of Multilevel TPA, enabling the sequential analysis of vibration transmission across hierarchical structural levels.

The simulation-based TPA methodology was validated by comparing contribution results from a non-reduced dual assembly with the analytical path contributions of a one-dimensional multi–mass–spring system. The agreement was excellent, with discrepancies typically below 0.1%.

Using a structural example of the Finite Element model of a two story building, the studied CMS methods were benchmarked to assess the balance between computational efficiency and numerical accuracy. The benchmark results confirm the fixed-interface methods, Craig-Bampton and the novel Fixed-dual Craig-Bampton as the most suitable CMS strategies for numerical TPA, alongside the non-reduced primal and dual approaches.

However, these results are strongly case-dependent and cannot be regarded as generally valid for all problems, especially as complexity increases. This application should therefore be seen as a first step to explore the trade-off between computational efficiency and accuracy of CMS methods for TPA; more in-depth studies are needed, varying model parameters such as the domain type (e.g., replacing shells with solid elements or acoustic cavities), the component mesh density and interface-node ratio, and the boundary conditions applied to the components (e.g., with or without full rigid-body constraint), among other variables. In parallel, additional metrics should be introduced to assess when CMS methods are more efficient than their non-reduced counterparts. For example, a break-even point in terms of the number of harmonic-analysis iterations, the reduction in computation time per iteration, or condensed indicators that combine CPU time and RAM usage to quantify the accuracy–efficiency balance.

The Transfer Path Analysis was conducted in one-level and in multilevel procedures and the results were compared. The study demonstrated the effectiveness of multilevel TPA in identifying critical transmission paths and substructures, adding a better understanding of the vibration transmission throughout the assembly.

Finally, two distinct families of TPA were explored: displacement-based (primal) and force-based (dual). The displacement-based TPA formulation, analogous to *transmissibility TPA* schemes, conducted using the Craig-Bampton reduction, offers a different interpretation of the contribution results in comparison to the force-based TPA, relatable to *classical TPA*, represented by the Fixed Dual Craig-Bampton method.

This distinction in contribution results, arising from the two different types of prescribed loading conditions, naturally raises the question of which interpretation offers better guidance for reducing vibration transmission. The force-based TPA procedure, represented by the dual approach and the novel Fixed Dual Craig–Bampton method, is consistent with classical and component-based TPA, thereby highlighting the relevance of the newly developed CMS formulation and facilitating experimental validation of the simulation results.

In contrast, the u-TPA methodology corresponds to transmissibility-based TPA, but its requirement to fix all non-prescribed active interfaces for each interface under study severely limits its experimental validation and makes it considerably less practical than the f-TPA counterpart.

To conclude, the main limitations of the TPA methodology presented in this work are: (1) in its current form it is restricted to purely structural analyses (although an extension to a vibro-acoustic framework for simultaneous structure-borne and airborne noise tracing is under development); (2) by adopting a force-based TPA formulation, the dual methods using Lagrange multipliers are constrained to conforming and paired meshes and are generally less efficient than their primal counterparts; (3) multilevel TPA can become cumbersome and difficult to manage when many interfaces are involved; and (4) some CMS methods can be incompatible with interface conditions (damping, external forces), which might make them impractical in specific engineering problems.

CRediT authorship contribution statement

Said El Kadmiri Pedraza: Writing – original draft, Validation, Software, Methodology, Investigation, Formal analysis, Data curation, Conceptualization. **Hans Peter Monner:** Supervision, Project administration, Funding acquisition. **Stephan Algermissen:** Supervision, Project administration, Funding acquisition.

Declaration of generative AI and AI-assisted technologies in the writing process

During the preparation of this work the authors used *chatGPT* in order to improve the quality of the scientific writing, providing a better readability and language for the work. The AI-assisted technology was used solely for the purpose of text writing, and not for content creation. After using this service, the authors reviewed and edited the content as needed and take full responsibility for the content of the published article.

Funding sources

This work was supported by the European Union's Horizon Europe programme *IN-NOVA MSCA Doctoral Network* under the Marie Sklodowska-Curie grant agreement number 101073037.

Declaration of competing interest

The authors declare that they have no known competing financial interests or personal relationships that could have appeared to influence the work reported in this paper.

Data availability

The authors do not have permission to share data.

References

[1] Acri A, Offner G, Nijman E, Rejlek J. Substructuring of multibody systems for numerical transfer path analysis in internal combustion engines. Mech Syst Signal Process 2016;79:254–70.
[2] Allen MS, Rixen D, van der Seijs M, Tiso P, Abrahamsson T, Mayes RL. Substructuring in engineering dynamics, vol. 594. Cham: Springer International Publishing; 2020.
[3] Atalla N, Sgard F. Finite element and boundary methods in structural Acoustics and vibration: chapter 6: interior structural acoustic coupling. Baton Rouge, UNITED STATES: Taylor & Francis Group; 2015.
[4] Jetmundsen B, Bielawa RL, Flannelly WG. Generalized frequency domain substructure synthesis. J Am Helicopter Soc 1988;33:55–64.
[5] Craig RR, Bampton MCC. Coupling of substructures for dynamic analyses. AIAA J 1968;6(7):1313–9.
[6] de Klerk D, Rixen DJ, Voormeeren SN. General framework for dynamic substructuring: history, review and classification of techniques. AIAA J 2008;46(5):1169–81.
[7] El Kadmiri Pedraza S, Algermissen S, Monner HP. Development and comparative analysis of novel component mode synthesis methods for structural and acoustic applications. In: Electronica EAADOCUMENTAACUSTICA, editor. Forum Acusticum Euronoise. Malaga: Acta Acustica; 2025.
[8] Franco JA, Botelho RM, Christenson RE. Controls based hybrid sub-structuring approach to transfer path analysis. In: Allen M, Mayes RL, Rixen D, editors. Dynamics of coupled structures, volume 4. Cham: Springer International Publishing; 2016. p. 15–24.
[9] Gruber FM, Rixen DJ. Evaluation of substructure reduction techniques with fixed and free interfaces. Stroj Vestn J Mech Eng 2016;62(7–8):452–62.
[10] Guo R, Wang MJ, Zhou SQ, Qiu S. Numerical investigation of a two-stage serial vibration isolation system using frequency response function based substructuring method. Adv Mech Eng 2017;9.
[11] Haeussler M, Kobus DC, Rixen DJ. Parametric design optimization of e-compressor NVH using blocked forces and substructuring. Mech Syst Signal Process 2021;150:107217.
[12] Kim JG, Nam KU, Kang YJ. Evaluation of noise transfer path contributions using virtual springs with infinite stiffness. Appl Acoust 2021;178:107991.
[13] Kim SJ, Lee SK. Prediction of interior noise by excitation force of the powertrain based on hybrid transfer path analysis. Int J Automot Technol Oct 2008;9:577–83.
[14] Maia NMM, Silva JMM, Ribeiro AMR. The transmissibility concept in multi-degree-of-freedom systems. Mech Syst Signal Process 2001;15(1):129–37.
[15] Morgan JA, Pierre C, Hulbert G. Forced response of coupled substructures using experimentally based component mode synthesis. AIAA J 1997;35:334–9.
[16] Pasch G, Jacobs G, Berroth J. Numerical transfer path analysis for NVH system-simulation models. IOP Conf Ser Mater Sci Eng Feb 2021;1097(1):012008.
[17] R. H. MacNeal. A hybrid method of component mode synthesis. Comput Struct 1971;1(4):581–601.
[18] Rixen DJ. A dual craig–bampton method for dynamic substructuring. J Comput Appl Math 2004;168(1–2):383–91.
[19] Rubin S. Transmission matrices for vibration and their relation to admittance and impedance. J Eng Ind Feb 1964;86(1):9–21.
[20] Rubin S. Improved component-mode representation for structural dynamic analysis. AIAA J 1975;13(8):995–1006.
[21] Van der Auweraer H, Mas P, Dom S, Vecchio A, Janssens K, Van de Ponseele P. Transfer path analysis in the critical path of vehicle refinement: the role of fast, hybrid and operational path analysis. SAE Tech Pap May 2007:2352–2367. ISSN 0148-7191.
[22] van der Seijs MV, de Klerk D, Rixen DJ. General framework for transfer path analysis: history, theory and classification of techniques. Mech Syst Signal Process 2016;68-69:217–44.
[23] Wischmann S, Pasch G, Berroth J, Jacobs G. Acoustic optimization of a power take-off gear box using numerical transfer path analysis. IOP Conf Ser Mater Sci Eng 2021;1097(1):012012.
[24] Woller J, Lein C, Zeidler R, Beitelschmidt M. A numerical study of the structure-borne sound transmission of a bogie. Civ Comp Proc 2016;110.